



Trabecular organization of the proximal femur in *Paranthropus robustus*: Implications for the assessment of its hip joint loading conditions



Marine Cazenave ^{a,*}, Anna Oettlé ^b, Travis Rayne Pickering ^{c,d,e}, Jason L. Heaton ^{f,d,e},
Masato Nakatsukasa ^g, J. Francis Thackeray ^d, Jakobus Hoffman ^h, Roberto Macchiarelli ^{i,j}

^a Skeletal Biology Research Centre, School of Anthropology and Conservation, University of Kent, Canterbury, UK

^b Department of Anatomy and Histology, Sefako Makgatho Health Sciences University, Ga-Rankuwa, Pretoria, South Africa

^c Department of Anthropology, University of Wisconsin, Madison, USA

^d Evolutionary Studies Institute and School of Geosciences, University of the Witwatersrand, Johannesburg, South Africa

^e Plio-Pleistocene Palaeontology Section, Department of Vertebrates, Ditsong National Museum of Natural History (Transvaal Museum), Pretoria, South

Africa

^f Department of Biology, Birmingham-Southern College, Birmingham, USA

^g Laboratory of Physical Anthropology, Department of Zoology, Graduate School of Science, Kyoto University, Kyoto, Japan

^h South African Nuclear Energy Corporation SOC Ltd, Pelindaba, South Africa

ⁱ Département Homme & Environnement, UMR 7194 CNRS, Muséum national d'Histoire naturelle, 75116, Paris, France

^j Unité de Formation Géosciences, Université de Poitiers, Poitiers, France

ARTICLE INFO

Article history:

Received 5 June 2020

Accepted 28 January 2021

Available online xxx

Keywords:

Trabecular pattern

Proximal femur

Hominin biomechanics

X-ray microtomography

Swartkrans

South Africa

ABSTRACT

Reconstruction of the locomotor repertoire of the australopiths (*Australopithecus* and *Paranthropus*) has progressively integrated information from the mechanosensitive internal structure of the appendicular skeleton. Recent investigations showed that the arrangement of the trabecular network at the femoral head center is biomechanically compatible with the pattern of cortical bone distribution across the neck, both suggesting a full commitment to bipedalism in australopiths, but associated with a slightly altered gait kinematics compared to *Homo* involving more lateral deviation of the body center of mass over the stance limb. To provide a global picture in *Paranthropus robustus* of the trabecular architecture of the proximal femur across the head, neck and greater trochanter compartments, we applied techniques of virtual imaging to the variably preserved Early Pleistocene specimens SK 82, SK 97, SK 3121, SKW 19 and SWT1/LB-2 from the cave site of Swartkrans, South Africa. We also assessed the coherence between the structural signals from the center of the head and those from the trabecular network of the inferolateral portion of the head and the inferior margin of the neck, sampling the so-called vertical bundle, which in humans represents the principal compressive system of the joint. Our analyses show a functionally related trabecular organization in *Pa. robustus* that closely resembles the extant human condition, but which also includes some specificities in local textural arrangement. The network of the inferolateral portion of the head shows a humanlike degree of anisotropy and a bone volume fraction intermediate between the extant human and the African ape patterns. These results suggest slight differences in gait kinematics between *Pa. robustus* and extant humans. The neck portion of the vertical bundle revealed a less biomechanically sensitive signal. Future investigations on the australopith hip joint loading environment should more carefully investigate the trabecular structure of the trochanteric region and possible structural covariation between cortical bone distribution across the neck and site-specific trabecular properties of the arcuate bundle.

© 2021 Elsevier Ltd. All rights reserved.

* Corresponding author.

E-mail address: marine.cazenave4@gmail.com (M. Cazenave).

1. Introduction

1.1. Background

Based on the observation by von Meyer (1867) on the original work by Culmann (1866), who firstly noted that the orientation of the trabecular struts within the human proximal femur was remarkably similar to the internal compressive and tensile stress lines of a crane (i.e., similar to a cantilevered beam), Wolff (1892) went on to state that trabecular bone architecture follows the principal stress trajectories generated from external loads—a theory known as Wolff's law, otherwise referred to as the trajectory hypothesis (Ruff et al., 2006). Although these first observations were formulated in a strict mathematical sense that has since been discredited (Ruff et al., 2006; Kivell, 2016), in vivo experimental studies have demonstrated that, within the geometric limits imposed by a phylogenetically determined adaptive bauplan and the influence of a number of biological (metabolic) factors (e.g., Lovejoy et al., 1999; Judex et al., 2004; Demissie et al., 2007; Havill et al., 2007, 2010; Bonewald and Johnson, 2008; O'Neill and Dobson, 2008; Cunningham and Black, 2009; Estrada et al., 2012; Reissis and Abel, 2012; Wallace et al., 2012, 2020; Medina-Gomez et al., 2018; Hou et al., 2020), variation in cortical bone distribution and site-specific arrangement of the trabecular network respond to the mechanical loading environment to resist local stresses (e.g., Lanyon, 1973; Skerry and Lanyon, 1995; Biewener et al., 1996; Guldberg et al., 1997; Mori et al., 2003; Mittra et al., 2005; Pontzer et al., 2006; Carlson and Judex, 2007; Chang et al., 2008; Polk et al., 2008; Barak et al., 2011; Wallace et al., 2013; Cresswell et al., 2015; Vera et al., 2020). These studies support the more general concept of 'bone functional adaptation' (Ruff et al., 2006).

Even though the endostructural arrangement of the proximal femur is more complex and less straightforward than assumed by the first mechanical models (e.g., Fajardo et al., 2007; Ryan and Walker, 2010; Shaw and Ryan, 2012), several studies have successfully investigated its patterns of cortical and trabecular bone organization to identify behavioral signals in humans and other primates. Indeed, the assessment of the trabecular organization of the femoral head in taxa displaying different locomotor behaviors has provided evidence for structural differences across locomotor groups (Fajardo and Müller, 2001; MacLatchy and Müller, 2002; Ryan and Ketcham, 2002a, b, 2005; Ryan and Krovitz, 2006; Saparin et al., 2011; Ryan and Shaw, 2012, 2015; Raichlen et al., 2015; Ryan et al., 2018; Tsegai et al., 2018a; Georgiou et al., 2019). Similarly, the asymmetrical distribution of cortical bone thickness within the femoral neck compartment has been shown to characterize bipedal humans and quadrupedal primates, reflecting their distinct stereotypical loadings at the hip joint (Ohman, 1993; Ohman et al., 1997; Rafferty, 1998; Pina et al., 2019). Accordingly, the quantitative assessment of how internal bone structure of the proximal femur varies can be used to infer locomotion-related functional demands in extinct taxa.

The reconstruction of the positional and locomotor repertoires of the australopiths (the term used here to refer to the taxa *Australopithecus* and *Paranthropus*) has progressively integrated information from the mechanosensitive internal structure of the hip joint to the classical studies on the outer skeletal morphology (e.g., Lovejoy, 1988, 2005; Ohman, 1993; Ohman et al., 1997; Macchiarelli et al., 1999, 2001; Ruff et al., 1999, 2016, 2020; Lovejoy et al., 2002; Volpati, 2007; Ruff and Higgins, 2013; Claxton, 2018; Ryan et al., 2018; Cazenave et al., 2019a; Georgiou et al., 2020).

Compared to the condition displayed by the extant great apes, australopiths show an absolutely thinner superior cortex of the femoral neck relative to the inferior cortex. This pattern is thought

to reflect relatively and absolutely reduced stresses across the superior neck due to the action of the gluteal abductors producing compressive forces that counteract tensile stresses engendered by bending of the proximal femur during weight bearing (Lovejoy, 1988, 2005; Ohman et al., 1997; Rafferty, 1998; Lovejoy et al., 2002; Ruff and Higgins, 2013; Ruff et al., 2016, 2020; Claxton, 2018; Friedl et al., 2019; Cazenave et al., 2019a). The combination of a humanlike superoinferior asymmetry in cortical bone distribution at the base of the neck, and less asymmetry than humans at mid-neck, has been interpreted as a full commitment to terrestrial bipedalism in australopiths. However, this is associated with slightly altered gait kinematics compared to *Homo*, involving a more lateral deviation of the body center of mass over the stance limb (Ruff and Higgins, 2013; Ruff et al., 2016, 2020).

Recently, three additional defining features have been identified by Cazenave et al. (2019a) in the femoral neck compartment of *Paranthropus robustus*. The first, shared with humans but not with *Pan*, consists in a decrease in asymmetry of the superior/inferior cortical thickness ratio across the neck from the base to the head-neck junction. Chimpanzees show an opposite pattern. The other two features, so far uniquely found in *Pa. robustus*, consist in an accentuated contrast between the relatively thicker anterior and the thinner posterior walls, and in a more marked lateral-to-medial thinning of both cortices compared to extant humans and chimpanzees. Whether these features also characterize the femoral neck of *Australopithecus* remains unknown (Cazenave et al., 2019a).

The signal from the trabecular bone organization of the proximal femur in australopiths, so far limited to the head compartment (Ryan et al., 2018; Georgiou et al., 2020), is biomechanically consistent with that provided by cortical bone arrangement at the neck. In a sample of six *Australopithecus africanus* and four *Pa. robustus* specimens, Ryan et al. (2018) showed that trabecular network fabric at the center of the head is more similar to that of extant and fossil humans than of extant apes, thus indicating that australopiths walked with humanlike hip kinematics, including a more limited range of habitual hip joint postures (e.g., a more extended hip; cf. Kozma et al., 2018). In this respect, no difference has been found between the femoral head endostructural signals provided by *A. africanus* and *Pa. robustus* (Ryan et al., 2018). However, a different picture has recently been suggested by Georgiou et al. (2020) in their comparative analysis of the whole trabecular bone distribution of the femoral head in two specimens from Sterkfontein Caves, South Africa. They identified distinct patterns of trabecular organization between an *A. africanus* specimen exhibiting a modern humanlike trabecular distribution, and in another specimen (attributed to either *Homo* sp. or *Pa. robustus*) showing a distribution more similar to nonhuman hominoids. Georgiou et al. (2020) suggested that the trabecular pattern within the latter specimen reflects habitual bent-hip postures, typically used during climbing. Their findings, still to be corroborated by the analysis of other specimens, point to possible locomotor differences between *Australopithecus* and later hominins in South Africa (Georgiou et al., 2020).

Most of the postcranial elements forming the *Pa. robustus* hypodigm are fragmentary and isolated, which complicates the task of confidently reconstructing the locomotor repertoire of this extinct hominin. However, the Early Pleistocene cave site of Swartkrans (Brain 1981) has yielded an assemblage of five variably preserved proximal femora (SK 82, SK 97, SK 3121, SKW 19 and SWT1/LB-2), all attributed on the basis of comparative morphology to *Pa. robustus* (Susman et al., 2001; Pickering et al., 2012; Ruff and Higgins, 2013). So far, this assemblage represents the most appropriate material to identify in this taxon a nonidiosyncratic signal from the inner bony conformation of the proximal femur reflecting the adaptive hip joint loading conditions.

1.2. Aims of the study and predictions

This study builds on a previous analysis of cortical bone thickness proportions and distribution across the femoral neck based on the X-ray microtomographic data of four *Pa. robustus* from the Swartkrans assemblage (Cazenave et al., 2019a). Here we apply 2D and 3D techniques of virtual imaging (i) to provide a global comparative picture of the structural organization of the medial and lateral systems forming the trabecular architecture of the whole proximal femur across its three major compartments, i.e., the head, the neck and the greater trochanter (Aiello and Dean, 1990; Levangie and Norkin, 2005; Kapandji, 2011), by also using unreported evidence from the relatively well-preserved specimen SWT1/LB-2 (Pickering et al., 2012); (ii) to build upon the analysis of Ryan et al. (2018) on the trabecular bone properties at the center of the femoral head by sampling the so-called vertical bundle at the inferolateral portion of the head, which in humans represents the principal compressive system of the joint (Levangie and Norkin, 2005; Kapandji, 2011); and (iii) to provide the first evidence of site-specific trabecular organization of the portion of the same vertical bundle close to the inferior margin of the neck.

In humans, the bundles forming the so-called principal trabecular system of the ilium converge towards the hip joint, where they uninterruptedly flow into the vertical and arcuate bundles transferring the loads to the proximal femur (Correnti, 1955; Aiello and Dean, 1990; Macchiarelli et al., 1999, 2001; Levangie and Norkin, 2005; Kapandji, 2011). With a few minor textural distinctions probably reflecting a “slightly altered gait kinematics compared with *Homo* and modern humans” (Ruff and Higgins, 2013: 523), the australopith iliac bone shows a globally humanlike trabecular architecture (Macchiarelli et al., 1999, 2001). The multidirectional loads acting at the human hip joint are managed by a structurally heterogeneous compressive-tensile trabecular organization, likely reflecting the one-legged stance phase of bipedal gait and the wide ranges of motion of abduction and adduction (Beaupré et al., 1990; Tsubota et al., 2002; Jang and Kim, 2008). The African apes are primarily terrestrial quadrupeds, but also engage in a variety of locomotor activities on arboreal substrates, including climbing, bridging, and below-branch suspension (Hunt, 1991; Doran, 1993a,b, 1997; Remis, 1995; Crompton et al., 2010). This more diverse loading environment relative to the human condition would elicit more diverse hip joint angles (Pontzer et al., 2014; Ryan et al., 2018). Accordingly, we predict that the *Pa. robustus* proximal femur displays a vertical and an arcuate bundle globally forming a humanlike, not ape-like, primary compressive and tensile trabecular system, respectively. This is probably associated with some locally distinct textural characteristics.

At the proximal femur, the cancellous bone network is less anisotropic in African apes than in humans (Ryan et al., 2018; Georgiou et al., 2019). In australopiths, both a humanlike anisotropic trabecular structure and a primate-like pattern of robust trabecular bone have been identified at the center of the femoral head (Ryan et al., 2018). Thus, our second expectation is that, at least across the femoral head, the vertical and the arcuate trabecular bundles show a structural organization distinguishable from both the human and the African ape conditions in terms of local density and degree of anisotropy. In their analysis of the trabecular architecture of the femoral neck in some nonhuman primates displaying diverse locomotor modes, Fajardo et al. (2007) did not observe clear differences in structural organization. Similarly, in comparatively assessing the trabecular pattern at the ilium and the femoral neck in a bipedally trained Japanese macaque (Sansuke) and in wild representatives of the same taxon, Volpato (2007) found that, while Sansuke's ilium deviated in many ways from the nontrained macaque pattern, the inner organization of its

femoral neck did not differ from that typical wild pattern, including the morphology of the vertical bundle. In another study, Skedros and Baucum (2007) found that trabecular tracts were similarly nonorthogonal in the femoral neck of both humans and chimpanzees, while orthogonal intersections were expected in the latter. Therefore, we expect that, differently from the femoral head pattern, in *Pa. robustus* the endostructural organization of the trabecular network across the femoral neck is poorly distinguishable from the general pattern found in extant humans and African apes.

2. Materials and methods

2.1. Materials

Fossil specimens The sample of *Pa. robustus* partial proximal femora, all from the Pleistocene cave deposits of Swartkrans, South Africa, includes the adult specimens SK 82, 97, 3121, SKW 19 and SWT1/LB-2, all from the right side (Fig. 1). SK 82, SK 97 and SKW 19 (Robinson, 1972; Susman et al., 2001) come from the Hanging Remnant of Member 1, while SWT1/LB-2 (Pickering et al., 2012) derives from the Lower Bank of the same member, whose chronology globally ranges between 2.31 and 1.64 Ma (Curnoe et al., 2001; Balter et al., 2008; Herries et al., 2009; Pickering et al., 2011, 2019; Gibbon et al., 2014). Only specimen SK 3121 (Susman et al., 2001) comes from the later Member 2 breccia block, the dating of which has proved more problematic. However, on the basis of U–Pb dates (Balter et al., 2008; see also; Herries et al., 2009; Gibbon et al., 2014), its chronology could be expected to range between 1.36 and 1.1 Ma (Pickering et al., 2019). This is compatible with the biochronology indicated by Vrba (1975) and Delson (1988).

Information on degree of preservation, and on the outer morphological characteristics of all specimens except SKW 19, has recently been provided by Cazenave et al. (2019a). SKW 19 represents a right femoral head (maximum diameter = 31.9 mm) preserving only a minor portion (8–10 mm) of the neck (Susman et al., 2001). The fovea capitis is large but relatively shallow, with a prominent rim. The head–neck junction is marked, probably because of the recent fusion of the secondary ossification center at this metaphysis, indicating that this fossil represents a young adult. Discovered by C.K. Brain some time after 1970, SKW 19 has been assigned to *Pa. robustus* based on its proportions and because of anteroposterior compression expressed by its preserved neck portion (Susman et al., 2001). Within the *Paranthropus* sample of proximal femora available so far, SKW 19 is considered to more likely represent a female because of its relatively small size (Susman et al., 2001; Pickering et al., 2012). Indeed, estimated body mass in this individual is 27.7–35.3 kg (Pickering et al., 2012; Ruff et al., 2018), which is smaller compared to SK 82 (37.1–45.3 kg), SWT1/LB-2 (37.1–45.8 kg), and especially of SK 97 (43.2–53.8 kg), all three commonly considered to be probably males (Susman et al., 2001; Pickering et al., 2012), but comparable to the body mass of assessed for SK 3121 which has estimated values ranging between 24.1 and 30.0 kg (Pickering et al., 2012; Ruff et al., 2018).

The specimens SK 82, 97, 3121, and SWT1/LB-2 are housed at the Ditsong National Museum of Natural History, Pretoria, while SKW 19 is curated at the Evolutionary Studies Institute of the University of the Witwatersrand (Wits), Johannesburg.

Comparative materials We compared SK 82, 97, 3121, SKW 19 and SWT1/LB-2 to three samples representing extant humans, chimpanzees (*Pan troglodytes*) and gorillas (*Gorilla gorilla*).

The extant human sample includes 20 adult individuals (10 females and 10 males, aged 21–54 years) of African and European ancestry from the Dart skeletal collection at Wits ($n = 4$; Dayal



Figure 1. The five proximal femora of *Paranthropus robustus* from Swartkrans considered in this study. All specimens shown in anterior view.

et al., 2009), the McGregor Museum of Kimberley ($n = 5$; Morris, 1984), and the Pretoria Bone Collection at the Department of Anatomy of the University of Pretoria ($n = 11$; L'Abbé et al., 2005). Details on the composition of this diverse sample are provided in Table 1. In the description of the patterns of trabecular organization within each compartment of the proximal femur, we also used the radiographic records of 60 proximal femora, including adult individuals of both sexes from the Imperial Roman osteological collection of Isola Sacra, Rome (Macchiarelli and Bondioli, 2000), which are available from the Kent Data Repository (Cazenave et al., 2020). The *P. troglodytes* sample (Table 1) consists of 15 femora from eight wild, one probably wild, and six individuals of unknown origin. All specimens are adults from both sexes (8 females, 3 males and 4 unknown). They are housed at the Evolutionary Studies Institute at Wits ($n = 1$), the Japan Monkey Center at Inuyama, Japan ($n = 5$; Shimizu et al., 2002), and the Muséum national d'Histoire naturelle (MNHN) of Paris, France ($n = 9$). For description of the whole trabecular architecture, we also used the XCT-based images of seven adult proximal femora, all from captive individuals, from the Primate Research Institute, Kyoto University (Digital Morphology Museum, KUPRI; <http://dmm.pri.kyoto-u.ac.jp/dmm/WebGallery/index.html>) and the record from two wild

individuals from the MNHN collections recorded by SR- μ XCT at the beamline ID 17 of the European Synchrotron Radiation Facility (ESRF) of Grenoble (350 μm isotropic voxel size). However, because of the modest resolution of their records, such nine specimens were not included in the quantitative analyses.

The *G. gorilla* sample ($n = 10$) consists of five female and five male wild adults from Cameroon housed at the Powell-Cotton Museum, UK, whose image data (Table 1) have been kindly granted by M. Skinner and T. Kivell (University of Kent).

All specimens used in this study for comparison lack any macroscopic evidence of outer or inner alteration, nor were there obvious pathological defects.

2.2. Methods

Data acquisition and image processing All specimens used for quantitative analyses were imaged by X-ray microtomography (μ XCT).

Among the fossils, SK 82, 97, 3121 and SWT1/LB-2 were scanned between 2014 and 2017 at the microfocus X-ray tomography facility (MIXRAD) of the South African Nuclear Energy Corporation SOC Ltd (Necsa), Pelindaba, using Nikon XTH 225 ST

Table 1The extant human ($n = 20$), *Pan troglodytes* ($n = 15$) and *Gorilla gorilla* ($n = 10$) comparative samples.

| Taxon/Specimen | Sex | Age (years) | Ancestry/Provenance | Behavior/Subsistence/Condition | Collection ^b | Scan location ^c | Voxel size (μm) |
|----------------------------------|-----|-------------|---------------------|--------------------------------|-------------------------|----------------------------|------------------------------|
| Extant humans^a | | | | | | | |
| A X199 | M | 41 | Zulu | likely agropastoralist | DART | ESI | 50 |
| A 3X27 | M | 40 | Zulu | likely agropastoralist | DART | ESI | 50 |
| A 33X2 | M | 40 | Zulu | likely agropastoralist | DART | ESI | 70 |
| A 374X | F | 38 | Zulu | likely agropastoralist | DART | ESI | 67 |
| MMK X08 | M | 30–49 | Khoesan | hunter gatherer | McGM | ESI | 67 |
| MMK 2X3 | F | 44–54 | Khoesan | hunter gatherer | McGM | ESI | 70 |
| MMK 23X | F | 30–40 | Khoesan | hunter gatherer | McGM | ESI | 67 |
| MMK X36 | F | 32–52 | Khoesan | hunter gatherer | McGM | ESI | 70 |
| MMK 2X0 | F | 30–47 | Khoesan | hunter gatherer | McGM | ESI | 67 |
| X926 | M | 41 | European | likely sedentary | PBC | NECSA | 69 |
| 5X55 | M | 51 | European | likely sedentary | PBC | NECSA | 67 |
| 56X6 | M | 51 | European | likely sedentary | PBC | NECSA | 67 |
| 576X | F | 32 | African | NA | PBC | NECSA | 69 |
| 5X78 | F | 32 | African | NA | PBC | NECSA | 69 |
| 60X4 | F | 48 | European | likely sedentary | PBC | NECSA | 50 |
| 6X99 | M | 27 | African | NA | PBC | NECSA | 65 |
| 62X3 | F | 48 | European | likely sedentary | PBC | NECSA | 69 |
| 631X | M | 26 | African | NA | PBC | NECSA | 65 |
| X338 | F | 21 | European | likely sedentary | PBC | NECSA | 69 |
| 702X | M | 26 | African | NA | PBC | NECSA | 65 |
| <i>Pan troglodytes</i> | | | | | | | |
| Za 1355 | M? | A | NA | wild? | ESI | ESI | 42 |
| BT | F | 20 | NA | wild | JMC | NSM | 70 |
| M07 | F? | A | NA | wild | JMC | NSM | 70 |
| M08 | U | A | NA | wild | JMC | NSM | 70 |
| MU | M | 36 | NA | wild | JMC | NSM | 70 |
| PU | F | 23 | NA | wild | JMC | NSM | 70 |
| A12761 | F | A | Gabon | wild | MNHN | MNHN | 80 |
| ZM-AC_1950-194 | M | A | Congo | wild | MNHN | MNHN | 73 |
| ZM-AC_1899-17 | M | A | NA | NA | MNHN | MNHN | 80 |
| ZM-AC_1923-2497 | F? | A | NA | NA | MNHN | MNHN | 67 |
| ZM-AC_1933-81 | F | A | Gabon | wild | MNHN | MNHN | 73 |
| ZM-AC_1936-630 | F | A | NA | NA | MNHN | MNHN | 73 |
| ZM-AC_1947-149 | F | A | NA | NA | MNHN | MNHN | 66 |
| ZM-AC_1956-67 | F | A | NA | NA | MNHN | MNHN | 67 |
| ZM-AC_1966-332 | F | A | NA | NA | MNHN | MNHN | 73 |
| <i>Gorilla gorilla</i> | | | | | | | |
| CAMI_106 | M | A | Cameroon | wild | PCM | CBC | 75 |
| MER_95 | F | A | Cameroon | wild | PCM | CBC | 54 |
| MER_96 | F | A | Cameroon | wild | PCM | CBC | 48 |
| MER_135 | M | A | Cameroon | wild | PCM | CBC | 60 |
| MER_264 | M | A | Cameroon | wild | PCM | CBC | 58 |
| MER_300 | F | A | Cameroon | wild | PCM | CBC | 60 |
| MER_372 | M | A | Cameroon | wild | PCM | CBC | 63 |
| MER_729 | M | A | Cameroon | wild | PCM | CBC | 62 |
| MER_798 | F | A | Cameroon | wild | PCM | CBC | 48 |
| MER_856 | F | A | Cameroon | wild | PCM | CBC | 45 |

Abbreviations: A = adult; F = female; M = male; NA = information not available.

^a Following South African stipulations, one digit within each individual label has been replaced by an 'X', in order to keep individual identity confidential.^b DART = R.A. Dart skeletal collection at the University of the Witwatersrand, Johannesburg, South Africa; ESI = Evolutionary Studies Institute of the University of the Witwatersrand, Johannesburg, South Africa; JMC = Japan Monkey Center, Inuyama, Japan; McGM = McGregor Museum, Kimberley, South Africa; MNHN = Muséum national d'Histoire naturelle, Paris, France; PBC = Pretoria Bone Collection, Pretoria, South Africa; PC = Powell-Cotton Museum, Birchington-on-Sea, UK.^c CBC = Cambridge Biomatography Centre (Nikon XT 225 ST Metris scanner) in the Department of Zoology at the University of Cambridge, Cambridge, UK; ESI = microfocus X-ray tomography facility (Nikon XT H225/320L industrial XCT system) at the Evolutionary Studies Institute of the University of the Witwatersrand, Johannesburg, South Africa; MNHN = AST-RX: X-ray tomography technical platform (v|tome|x L 240-180 equipment) at the Muséum national d'Histoire naturelle, Paris, France; NECSA = MIXRAD microfocus X-ray tomography facility (Nikon XTH 225 ST Metris equipment) at the South African Nuclear Energy Corporation SOC Ltd, Pelindaba, South Africa; NSM = microfocus X-ray tomography facility (CT TXS320-ACTIS TESCO Co. equipment) at the National Science Museum, Tokyo, Japan.

(Metris) equipment according to the following parameters: 100 kV (SK 3121 and SWT1/LB-2) and 190 kV (SK 82 and SK 97) tube voltage; 0.10 mA (SK 3121 and SWT1/LB-2) and 0.12 mA (SK 82 and 97) tube current; and an angular increment of 0.36° between each projection (for a total of 1000 projections). The specimen SKW 19 was scanned in 2015 at the microfocus X-ray tomography facility of the Evolutionary Studies Institute at Wits using a Nikon metrology XT H225/320L industrial XCT system equipped with a microfocal X-ray tube according to the following parameters: 85 kV tube voltage, 0.10 mA tube current, and an angular increment of 0.12° (for a total of 3000 projections). The final volumes were

reconstructed with an isotropic voxel size ranging from 20 μm (SKW 19) to 79 μm (SK 82).

For the comparative samples, 11/20 extant human femora were also imaged at Necsa at resolutions ranging from 50 μm to 69 μm isotropic voxel size, while the remaining human specimens and one chimpanzee femur housed in Johannesburg were scanned at the X-ray microtomography facility at Wits at resolutions ranging from 42 μm to 70 μm isotropic voxel size. Nine *Pan* femora were scanned at resolutions ranging from 66 μm to 80 μm isotropic voxel size at the MNHN, and five at the National Science Museum of Tokyo, Japan, with an isotropic voxel size of 70 μm (details on the μ XCT

equipment are provided in Table 1). Finally, the *Gorilla* sample was scanned at the Cambridge Bioluminescence Centre in the Department of Zoology at the University of Cambridge, UK, with an isotropic voxel size ranging from 45 μm to 75 μm (Table 1).

By using the more complete SK 82 and SK 97 fossils as reference material, SK 3121, SKW 19 and SWT1/LB-2 were virtually rotated in Avizo v. 8.0.0 (Visualization Sciences Group Inc., Bordeaux) so that all were oriented in the same way. This procedure was more complicated in the case of SKW 19. However, intra- and interobserver tests run for orientation accuracy on each fossil specimen, and on one representative of each extant sample repeated twice by two independent observers, provided differences of less than 4%. The same protocol was used to virtually orient the comparative materials. Independently from their original side, all extant specimens were imaged as right femora by mirroring left femora when necessary.

Trabecular bone analyses The most complete fossils, SK 82 and SK 97, have been subject to some degree of taphonomic and diagenetic alteration, which constrained the choice of areas suitable for assessment of the trabecular network properties across the *Pa. robustus* assemblage used in this study (Fig. 2). Notably, the center of the head could not be confidently analyzed in all fossils, contrasting with the study performed by Ryan et al. (2018) on a sample of australopith proximal femora. Following various tests among independent observers (Cazenave, 2015, 2018a, b; Cazenave et al., 2015), we identified in the lower region of the so-called vertical bundle, which arises from the superior aspect of the head and radiates inferiorly to the medial cortex of the upper shaft, a cubic volume of interest (hVOI) located in the inferolateral portion of the femoral head which delivered a sufficiently well-preserved amount of trabecular bone suitable for structural analysis in all five fossils (Fig. 3). The vertical bundle belongs to the medial trabecular system. It forms the principal compressive system transmitting to the lower neck, then to the medial aspect of the

diaphysis, with the vertical compressive forces passing through the hip joint (Ward, 1838; Whitehouse and Dyson, 1974; Aiello and Dean, 1990; Miller et al., 2002; Levangie and Norkin, 2005; Jang and Kim, 2008; Kapandji, 2011). In all fossil and extant specimens, the center of the hVOI is positioned at a distance of 37% of the anteroposterior diameter from the posterior aspect of the femoral head; 17% of the mediolateral diameter from the lateral aspect; and 29% of the superoinferior diameter from the inferior aspect (Fig. 3). Its side corresponds to 20% of the mediolateral head diameter and, among the *Pa. robustus* specimens, it ranges in volume from 85 mm^3 to 173 mm^3 , in SKW 19 and SWT1/LB-2, respectively, which is smaller than the cubic VOI extracted by Ryan et al. (2018; estimated approximate range = 857–1643 mm^3). In our comparative samples, the hVOI ranges from 158 mm^3 to 562 mm^3 in extant humans, from 75 mm^3 to 169 mm^3 in *Pan*, and from 263 mm^3 to 708 mm^3 in *Gorilla*.

In SK 82, 97, 3121 and SWT1/LB-2 (the fossils preserving at least a portion of the neck compartment), we also explored the possibility of assessing an homologous cubic VOI (nVOI) within the vertical bundle close to the inferior margin of the neck, which in australopiths and humans typically bears a thicker cortex compared to the superior margin (Ohman et al., 1997; Lovejoy et al., 2002; Ruff and Higgins, 2013; Ruff et al., 2016; Cazenave et al., 2019a). In the four fossils, an area preserving enough trabecular network has been identified at the mid-neck, at ca. 50% of the anteroposterior neck diameter (Fig. 3), where the nVOI's side has been set in each specimen at 17% of the maximum superoinferior height of the mid-neck. However, even if SK 82 shows a relatively greater amount of trabecular bone (Fig. 2), a reliable assessment of its textural properties is not possible in this specimen because of a noisy signal due to network discontinuities and matrix filling intertrabecular spaces. Accordingly, the analysis was limited to SK 97, 3121 and SWT1/LB-2, where the nVOI ranges from 39 mm^3 (in SK 3121), to 145 mm^3 (in SK 97). In the comparative samples, the

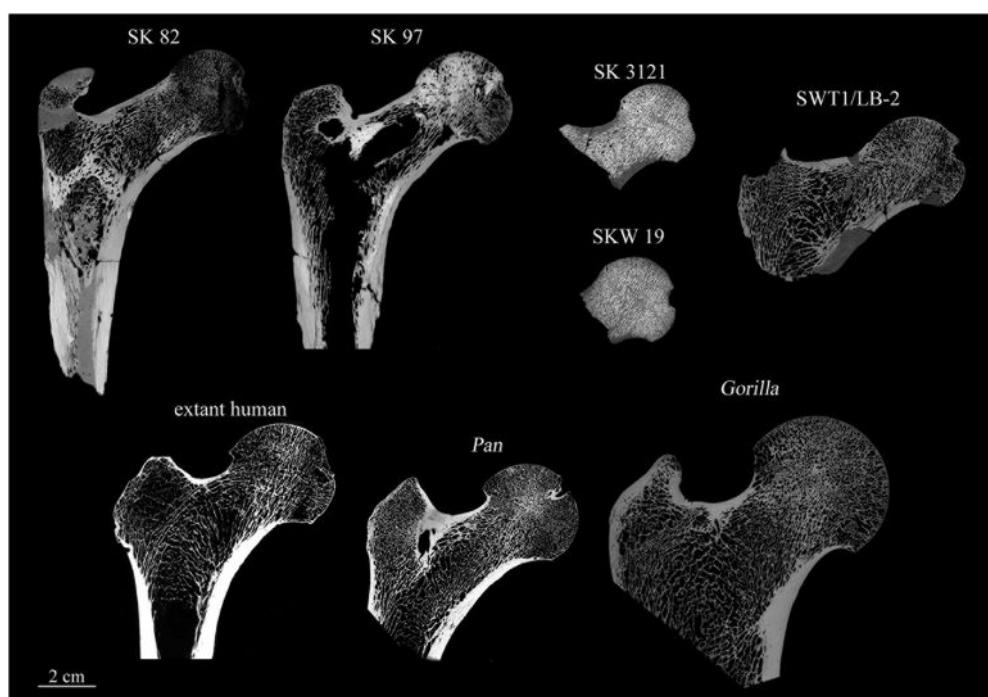


Figure 2. μXCT -based virtual coronal sections through the femoral head center showing the degree of inner preservation and the trabecular organization of the five proximal femora of *Paranthropus robustus* from Swartkrans (SK 82, SK 97, SK 3121, SKW 19 and SWT1/LB-2) compared to an extant human, a *Pan troglodytes* and a *Gorilla gorilla* representative.

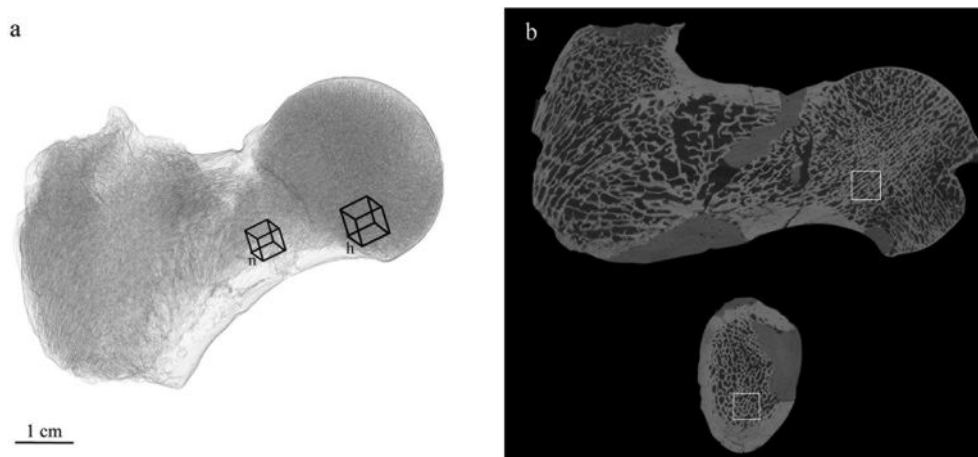


Figure 3. a) Position, orientation and volumetric proportions of the two cubic volumes of interests (VOIs) sampling the trabecular vertical bundle at the inferolateral portion of the femoral head (hVOI) and at the inferior margin of the femoral neck (nVOI). b) Virtual coronal slice through the center of the hVOI (upper) and virtual anteroposterior slice through the center of the nVOI (lower). The μ XCT-based 3D virtual rendering of the lateral view in semitransparency (a) and the two virtual slices (b) illustrate the *Paranthropus robustus* specimen SWT1/LB-2.

nVOI ranges from 56 to 271 mm³ in extant humans, from 16 to 101 mm³ in *Pan*, and from 78 to 266 mm³ in *Gorilla*.

The hVOI and nVOI were binarized into bone and nonbone using the 'half maximum height' (HMH) quantitative iterative thresholding method (Spoor et al., 1993) and the region of interest protocol (ROI-Tb; Fajardo et al., 2002) by taking repeated measurements on different slices of the virtual stack by using ImageJ (Schneider et al., 2012). Due to the biasing effects of a nonspherical VOI (Ketcham and Ryan, 2004) the largest centered sphere fitting completely within each cubic VOI was extracted in Quant3D (Ryan and Ketcham, 2002a). We measured: (i) the trabecular bone volume fraction (BV/TV, in %), given as the ratio of the number of bone voxels to the total number of voxels; and (ii) by using the star volume distribution (SVD) algorithm, the degree of anisotropy (DA), a fabric characteristic of trabecular bone assessed following Ryan and Ketcham (2002a) by dividing the eigenvalue representing the relative magnitude of the primary material axis of the bone structure (τ_1) by the eigenvalue representing the relative magnitude of the tertiary material axis of the bone structure (τ_3 ; see also Ryan and Walker, 2010; Shaw and Ryan, 2012). For each fossil specimen and one representative of each extant sample, the HMH was measured twice by two independent observers. The results of BV/TV and DA measured in Quant3D showed differences less than 5% and were not consistent in one direction.

Ryan et al. (2018) noted the technical issue of the use of μ XCT-based data obtained from different systems and scanning protocols implying variation in image resolution. This is of course the case in our study. To evaluate the extent of differences for BV/TV and DA with respect to the measures previously performed by Ryan et al. (2018), possibly reflecting differences among the scanning equipment and protocols, as a test-case we used SK 3121, scanned at Wits by Ryan et al. (2018) and reconstructed with an isotropic voxel size of 20 μ m (Ryan et al., 2018: Table 1). Following the analytical protocol described by Ryan et al. (2018) and using a VOI of 857 mm³ virtually extracted from its head center, we obtained a difference of 3.6% for BV/TV (0.56 vs. 0.54; Ryan et al., 2018: Table 2) and of 7.6% for DA (0.66 vs. 0.61; Ryan et al., 2018: Table 2), which we consider acceptable for the purposes of our study. In addition, we conducted a test to measure the possible effect on the results of the range of variation in spatial resolution of our record. By using Avizo, we downsampled the images of the hVOI and nVOI of specimen SK 3121 (originally scanned at 20 μ m) to obtain a spatial resolution of

79 μ m, which corresponds to the lowest resolution represented in our record of fossil specimens. Similarly, we used one human and one *Pan* specimen acquired respectively with a spatial resolution of 50 and 42 μ m, and downsampling the hVOIs to 70 and 80 μ m, respectively. We obtained the following differences: 2.2%, 0.3% and 2.5% for the BV/TV and 9.0%, 2.5% and 1.3% for the DA of the hVOI; 2.2%, 0.1% and 4.2% for the BV/TV and 2.7%, 10.2% and 0.0% for the DA of the nVOI of SK 2121, the human and *Pan* representatives, respectively. Even though the DA might be more affected than the BV/TV, we estimate that the effect of the range of variation of voxel size of our sample is acceptable for the purposes of our study. However, it should be noted that, when quantitatively analyzing the trabecular bone, optimizing spatial resolution has distinct advantages in quantification accuracy and image processing.

Besides other technical difficulties in assessing trabecular properties in fossil bone (Gross et al., 2014; Bishop et al., 2017), there are also several challenges associated with determining biomechanically 'homologous' VOIs across a sample (Maga et al., 2006; Kivell et al., 2011; Lazenby et al., 2011). In each individual forming our fossil and extant samples, both the hVOI and nVOI are systematically positioned within the vertical bundle, which is a homologous trabecular structure in hominid femora (Aiello and Dean, 1990; Lovejoy et al., 2002). However, we tested the possible influence on the results of a slightly different position of the hVOI in all five fossils. On a subsample of 15 randomly selected femora including five specimens from each comparative extant taxon (*Homo*, *Pan*, *Gorilla*), we measured the trabecular properties on a test tVOI of exactly the same hVOI's size positioned at the same anteroposterior and mediolateral level within the vertical bundle, but just superiorly adjacent to the original hVOI (Supplementary Online Material [SOM] Fig. S1). For the BV/TV and DA, the intra-class correlation coefficients measured in this subsample between the tVOI and the hVOI are 0.72 and 0.95, respectively, which indicates high similarity.

Statistical analyses Statistical analyses were performed using RStudio v. 1.2.5033 running with R v. 3.4.4 (R Core Team, 2018). Plots were generated using ggplot2 (Wickham, 2009). The significance of the differences among the taxa for BV/TV and DA was tested by the two-sample t-test via Monte Carlo sampling with 1000 permutations. The two variables were also tested for allometry using ordinary least squares regression through the R package lmodel2 (Legendre, 2018). Because body size information was not

systematically available for each individual representative of comparative samples, the superoinferior diameter of the femoral head was used as a proxy. Pairwise Wilcoxon rank sum tests were used to assess the significance of sex differences.

3. Results

3.1. Trabecular network architecture

The degree of inner preservation, and the trabecular bone architecture of the five fossil specimens from Swartkrans and of an extant human, a *Pan* and a *Gorilla* representative, are described in SOM S1 and shown in Figure 2. The major features forming the trabecular pattern of the adult human proximal femur described in Ward's classification (Ward, 1838; Whitehouse and Dyson, 1974; Aiello and Dean, 1990; Miller et al., 2002; Levangie and Norkin, 2005; Jang and Kim, 2008; Kapandji, 2011) are schematically shown using the common femur terminology in Figure 4 (see also Cazenave et al., 2020).

In SK 82, the vertical bundle arises from the superior aspect of the head and radiates inferolaterally towards the inferior cortex of the neck. The outline of its lower limit is slightly convex medially. A slightly inferiorly concave and relatively wide arcuate bundle is evident at the head-neck joint. This bundle, which forms the principal tensile structure of the lateral trabecular system (Ward, 1838; Whitehouse and Dyson, 1974; Aiello and Dean, 1990; Miller et al., 2002; Levangie and Norkin, 2005; Jang and Kim, 2008; Kapandji, 2011), crosses the superior portion of the neck and then bends inferiorly to join the lateral shaft cortex.

Apart from its faint appearance within the head, and a less arcuate outline, it fits the typical human morphology (Fig. 4). In its

lateral portion, the trabeculae forming this bundle are thicker and well oriented. Lateral to the base of the neck, a more closed network is noticeable. Inferiorly, the local impact of diagenetic changes accentuates the condition of likely thickened original trabeculae. The area below the crossing between the vertical and arcuate bundles, which in humans corresponds to 'Ward's triangle' (the 'zone of weakness' between principal compressive, secondary compressive and primary tensile trabeculae in the neck of femur; Levangie and Norkin, 2005: 367), is filled by a looser trabecular network but consists of relatively thicker struts than is typical in humans. Because of local damage, the trochanteric bundle is poorly distinguishable. However, near the base of neck, the presence of thickened superoinferiorly and mediolaterally projecting trabeculae displaying an arched outline is compatible with a humanlike so-called secondary compressive group bundle (Levangie and Norkin, 2005; Kapandji, 2011). Some elements of a bundle-like structure are also preserved within the greater trochanter, but the specimen is damaged in this area (Figs. 2 and 4).

The vertical and arcuate bundles are only partially preserved in SK 97. As in SK 82, the vertical bundle crosses the head and courses towards the inferior neck cortex. Across the head, it shows a slightly medially oriented convexity. The origin and first trait of the arcuate bundle are evident just below the fovea capitis. The arcuate bundle crosses the vertical bundle near the center of the femoral head. Its lateral extension goes through the superior portion of the neck. Despite damage resulting in textural discontinuities or local bone destruction, this bundle seems to terminate into the lateral diaphyseal cortex. The preserved network locally consists of relatively thick and well-oriented trabeculae. The trochanteric bundle is not appreciable; however, the greater trochanter is essentially filled by vacuolar-like trabecular bone (Figs. 2 and 4).

A slightly medially convex vertical bundle is well distinguishable in SK 3121. Conversely, the arcuate bundle is less expressed, with only poor evidence of intersection between the two structures. The origin of the arcuate bundle appears confined to the inferomedial head portion, just below the fovea capitis, where its trabeculae are abundant and well-oriented (Figs. 2 and 4).

In SKW 19, the preserved portions of the vertical and arcuate bundles trace the condition seen in SK 3121. The arcuate bundle is thinner than the vertical one and consists of oriented trabeculae essentially found in its inferomedial aspect (Figs. 2 and 4).

In SWT1/LB-2, the vertical, the arcuate and the trochanteric bundles are distinct. The vertical bundle is wide, rather dense, and inferomedially convex to a greater extent than observed in the other fossils, and also commonly seen in extant humans (Levangie and Norkin, 2005; Kapandji, 2011). Inferiorly, it extends laterally. Also the arcuate bundle is well defined all along its regularly arched and humanlike outline. This bundle can be traced from the inferomedial aspect of the head, just below the fovea capitis, across the upper portion of the neck, until the diaphyseal lateral cortex (even if the latter is not preserved). Its trabeculae are nearly universally thick and oriented. Similar to SK 82, the area below and lateral to the vertical-arcuate bundle crossing is the least dense and shows a loose trabecular network. However, in this case the trochanteric bundle is more structured than seen in SK 82 and consists of more distinct, thicker and oriented trabeculae. Conversely, because of local bone damage, the organization of the bundle-like structure of the greater trochanter is not fully appreciable, even if the region is filled by a relatively dense but poorly organized trabecular network. SWT1/LB-2 is also the only fossil among those examined here preserving partial evidence of the so-called secondary tensile trabecular system (Fig. 4). In the specimen, it is represented by relatively thick and obliquely oriented trabeculae departing from the medial aspect of the upper shaft and oriented towards the lateral diaphyseal cortex (Figs. 2, 4).

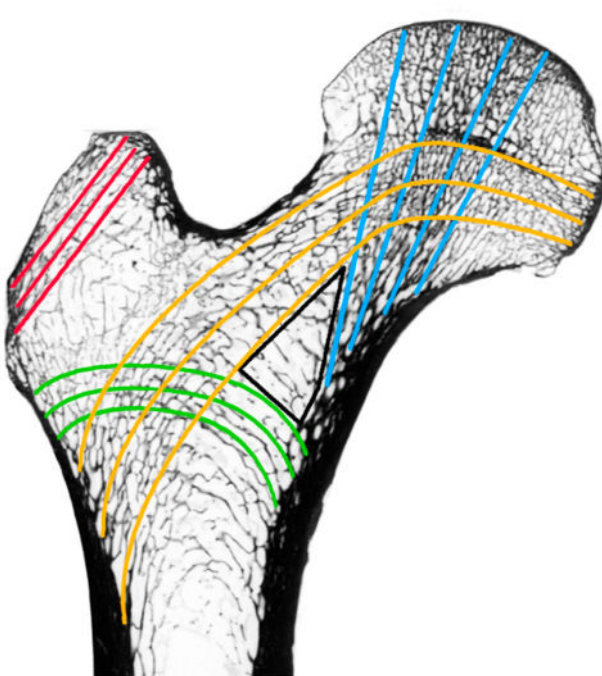


Figure 4. μXCT-based virtual coronal section of an extant human proximal femur (female, 32 years) showing the major systems of the trabecular architecture: the vertical bundle (in blue); the arcuate bundle (in yellow); the secondary compressive trochanteric bundle (in green); the bundle-like structure within the greater trochanter (red). The triangle-like structure (outline in black) below the crossing between the vertical and the arcuate bundles is the 'Ward's triangle' (Levangie and Norkin, 2005; Kapandji, 2011). (For interpretation of the references to color in this figure legend, the reader is referred to the Web version of this article.)

3.2. Trabecular network properties

Trabecular properties of the hVOI sampling the inferolateral portion of the femoral head vertical bundle (Fig. 3) in all five *Pa. robustus* specimens from Swartkrans and in the extant taxa (human, *Pan* and *Gorilla*) are shown in Figure 5 and Table 2. For the bone volume fraction (BV/TV), the values in the fossils range from 31.5%, in the relatively small-sized SKW 19, to 44.6%, in the larger SWT1/LB-2. The values of the two other relatively large individuals of this assemblage, SK 82 and SK 97, also exceed that of SK 3121, the other small-bodied individual. Bone volume fraction estimates in the fossils are significantly higher than those measured in our human comparative sample ($p = 0.03$), but significantly lower compared to *Pan* ($p = 0.003$) and *Gorilla* ($p = 0.004$), while the differences between the African apes are not significant ($p = 0.59$; SOM Table S1). For the degree of anisotropy (DA), the estimates of *Pa. robustus* (range = 2.56–3.70) do not differ from those of extant humans ($p = 0.12$) and *Gorilla* ($p = 0.32$), but they are significantly higher than measured in *Pan* ($p = 0.008$), the latter also significantly differing from extant humans ($p < 0.001$) and *Gorilla* ($p = 0.001$; Fig. 5; Table 2; SOM Table S1).

Among the fossil specimens, trabecular bone properties of the nVOI sampling the vertical bundle at the inferior mid-neck (Fig. 3) have only been assessed in SK 97, SK 3121 and SWT1/LB-2. Together with the values measured in the comparative samples, they are shown in Figure 5 and Table 2. For BV/TV, the *Pa. robustus* estimates (range = 50.4–57.3%) fall within the wide ranges of variation expressed by extant humans (17.3–77.2%), *Pan* (33.8–70.8%) and *Gorilla* (31.0–57.8%), which do not show significant differences (SOM Table S1). At this femoral neck site, *Pa. robustus* shows relatively low DA values (range = 3.39–4.99), which are closest to those of *Pan* (Table 2). Among the three fossils, SK 3121 displays the lowest bone volume fraction but the highest degree of anisotropy (Table 2). In the other extant taxa, the highest DA values have been found within the absolutely and relatively more variable extant

Table 2

Bone volume fraction (BV/TV, in %) and degree of anisotropy (DA) of the volume of interest sampling the trabecular vertical bundle at the inferolateral portion of the femoral head (hVOI; Fig. 3) and at the inferior margin of the femoral neck (nVOI; Fig. 3) in *Paranthropus robustus* from Swartkrans (SK 82, SK 97, SK 3121, SKW 19 and SWT1/LB-2) and in three comparative samples representing extant humans, *Pan troglodytes* and *Gorilla gorilla*. For each sample, sample size, the mean, the SD (in parenthesis), and the ranges are provided.

| Specimen/sample | hVOI | | nVOI | |
|-------------------------------------|------------|-------------|-------------|-------------|
| | BV/TV (%) | DA | BV/TV (%) | DA |
| <i>Paranthropus robustus</i> | 37.1 (5.3) | 3.23 (0.49) | (3.5) | (0.85) |
| SK 82 | 36.4 | 2.56 | n.a. | n.a. |
| SK 97 | 39.9 | 3.48 | 54.5 | 4.68 |
| SK 3121 | 33.1 | 3.55 | 50.4 | 4.99 |
| SKW 19 | 31.5 | 3.70 | n.a. | n.a. |
| SWT1/LB-2 | 44.6 | 2.86 | 57.3 | 3.39 |
| extant humans ($n = 20$) | 29.9 (6.4) | 4.40 (1.97) | 48.1 (13.5) | 6.07 (3.02) |
| | 17.5–43.2 | 2.19–8.73 | 17.3–77.2 | 2.52–12.99 |
| <i>Pan troglodytes</i> ($n = 15$) | 49.6 (7.2) | 2.23 (0.61) | 53.8 (10.3) | 4.80 (2.19) |
| | 34.2–60.4 | 1.37–3.64 | 33.8–70.8 | 1.60–7.56 |
| <i>Gorilla gorilla</i> ($n = 10$) | 51.5 (9.5) | 3.71 (1.07) | 47.4 (8.0) | 5.27 (1.32) |
| | 39.5–67.2 | 2.18–5.23 | 31.0–57.8 | 2.51–6.80 |

human sample (Table 2), whose average (6.07) is significantly higher than the value obtained for *Pan* ($p = 0.04$), but not in *Gorilla* ($p = 0.36$). Compared to the DA measured at the hVOI, at this site, the African apes do not differ significantly ($p = 0.11$; SOM Table S1).

4. Discussion

To face the complex set of posture- and locomotion-related forces acting at the hip joint, in humans the upper femur displays a structured and heterogeneous trabecular architecture (Aiello and Dean, 1990; Levangie and Norkin, 2005; Kapandji, 2011; Milovanovic et al., 2017; Cazenave et al., 2020). Together with the functional role played by cortical bone in carrying the loads at this

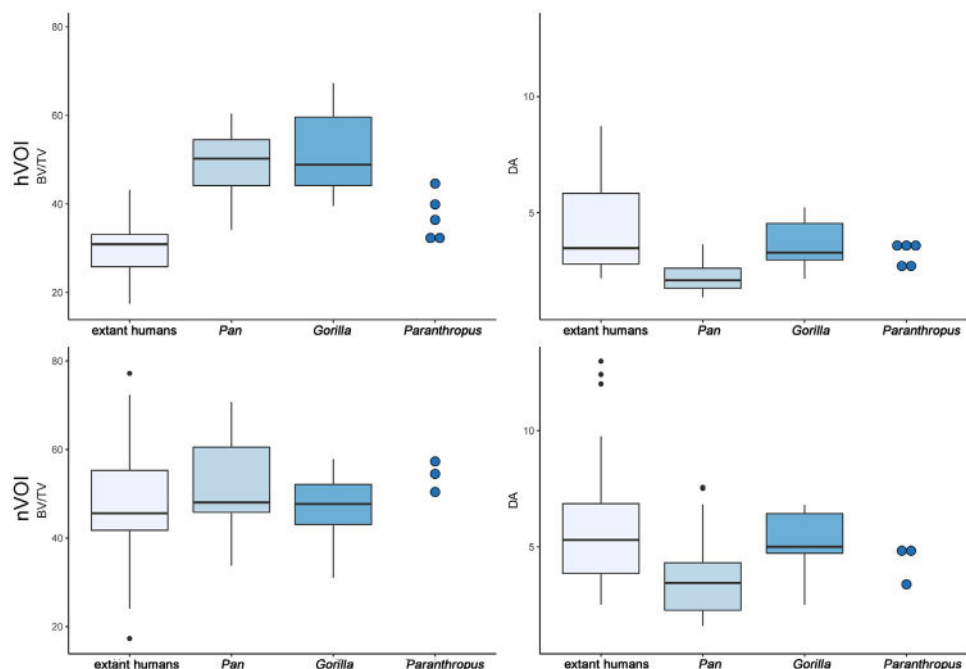


Figure 5. Boxplots of the median, standard deviation, minimum and maximum values (filled circles are outliers outside 1.5 times the interquartile range) of the bone volume fraction (BV/TV, in %) and degree of anisotropy (DA) of the volume of interest sampling the trabecular vertical bundle at the inferolateral portion of the femoral head (hVOI; Fig. 3) and at the inferior margin of the femoral neck (nVOI; Fig. 3) in *Paranthropus robustus* from Swartkrans (SK 82, SK 97, SK 3121, SKW 19 and SWT1/LB-2) and in three comparative samples representing extant humans, *Pan troglodytes* and *Gorilla gorilla*.

joint (Lotz et al., 1995; Crabtree et al., 2001; Levangie and Norkin, 2005), the trabecular bundles respond to stresses, which are mostly compressive and tensile, acting on the proximal femur, the areas where the bundles cross providing the greatest resistance to stress and strain. However, while some interspecific differences in the structural arrangement of the trabecular network of the hip joint contain a locomotor-specific functional signal, reflecting differences in site-specific loading conditions, i.e., the biomechanical environment (Levangie and Norkin, 2005; Kapandji, 2011), their immediate translation in terms of nature (e.g., compressive, tensile, shear), direction, frequency, and magnitude of such loads is not always clear (Tsegai et al., 2018a). For example, the trabecular architecture of the human proximal femur (extensively investigated because of its complex developmental pattern; see review in Milovanovic et al., 2017), has been shown to be not fully consistent at all sites ('fields') with the basic tenets of the 'trajectory hypothesis'. This evidence cautions against simple interpretations of trabecular bone adaptation in the anthropoid femoral neck (Fajardo et al., 2007; Skedros and Baucom, 2007; Sinclair et al., 2013; Milovanovic et al., 2017). Nonetheless, studies of the trabecular organization of the femoral head in a diversity of primate taxa displaying different locomotor behaviors provide evidence for structural differences in trabecular architecture across locomotor groups, where repetitive/stereotypical loading patterns are commonly associated with anisotropic trabecular networks, whereas heterogeneous/variable patterns are associated with isotropic networks (e.g., Fajardo and Müller, 2001; MacLatchy and Müller, 2002; Ryan and Ketcham, 2002a, b, 2005; Ryan and Krovitz, 2006; Ryan and Walker, 2010; Saparin et al., 2011; Ryan and Shaw, 2012, 2015; Shaw and Ryan, 2012; Raichlen et al., 2015; Ryan et al., 2018; Tsegai et al., 2018a; Georgiou et al., 2019).

Similarities in the basic distribution and directionality of the trabecular bone across the proximal femur exist among the extant hominids (e.g., Lovejoy et al., 2002; Fajardo et al., 2007; Georgiou et al., 2019). However, compared to the normal adult human trabecular pattern, *Pan* and *Gorilla* display a less organized and globally denser configuration. Indeed, in the African apes the poorly distinct trabecular systems, notably those forming the three so-called minor (accessory) systems (Levangie and Norkin, 2005; Kapandji, 2011), reveal a uniform network organization.

To facilitate the reconstruction of the hip joint loading conditions in *Pa. robustus*, we have extended the record available on the trabecular arrangement of the femoral head (Ryan et al., 2018; Georgiou et al., 2020) and cortical bone distribution of the neck (Ruff and Higgins, 2013; Cazenave et al., 2019a) by investigating the still poorly reported trabecular network organization across the entire proximal femur of this extinct hominin. For this, we used the entire assemblage of five specimens available so far from the Early Pleistocene cave site of Swartkrans (SK 82, 97, 3121, SKW 19 and SWT1/LB-2). Major analytical limitations were imposed by the incompleteness and by the variable degree of relative preservation of the fossils (notably, SK 3121 and SKW 19), as well as by the diverse quality of their site-specific inner signal (notably, in SK 97). Nonetheless, our results, which document for the first time the network arrangement within the neck compartment of three *Pa. robustus* specimens, have allowed the identification of structural features probably characterizing *Pa. robustus* with respect to extant humans and African apes.

According to our first expectation, the trabecular pattern of the proximal femur in *Pa. robustus* more closely resembles the extant human condition by showing a heterogeneous structure across the head, neck and greater trochanter compartments (while a relatively homogenous structure has been observed in all *Pan* and *Gorilla* specimens forming our sample, including those from the KUPRI website). However, it also shows some qualitative differences in

local textural arrangement absent or uncommon in extant humans and African apes (Fig. 6). Specifically, *Pa. robustus* shows (i) a variably marked medially convex (i.e., arched): vertical bundle, especially in its head portion, which is never expressed in the microtomographic and radiographic extant human samples used in this study (Fig. 6) but is present, for example, in the *A. africanus* specimens StW 311 and StW 501 (Ryan et al., 2018); (ii) an origin of the arcuate bundle, also noticeable in *A. africanus* (Ryan et al., 2018), confined to the head portion below the fovea capitis, while in our radiographic sample it reaches (44%), or even exceeds (10%), the level of the depression (Fig. 6); (iii) a looser appearance of the network in the so-called 'Ward's triangle', below the vertical and arcuate bundles crossing (Fig. 6). However, in contrast to the extant human pattern where increasing bone loss in this area is appreciable even in relatively young adults (in our radiographic sample [Cazenave et al., 2020], for example, in 100% of the individuals more than 25 years old), at this site the struts of the fan-shaped trochanteric bundle are thickened and well-oriented in *Pa. robustus* (notably in SWT1/LB-2; Fig. 6). This configuration, also displayed by *A. africanus* (e.g., StW 479; Ryan et al., 2018), differs from the poorly organized vacuolar network of all *Pan* and *Gorilla* specimens of our sample (Fig. 6); (iv) a proportionally greater amount of trabecular bone at the greater trochanter forming a network of intermediate texture and density between the loose human pattern (71% of the cases in our radiographic sample) and the denser honeycomb network typical of *Pan* and *Gorilla* (Fig. 6). Conversely, a vertical bundle which extends quite laterally along the inferior margin of the neck until the medial diaphyseal cortex does not appear to represent a unique australopith feature (for *A. africanus*, see Ryan et al., 2018; for *Australopithecus afarensis*, see Lovejoy et al., 2002). Such a feature might therefore mechanically correlate with the typically longer femoral neck shared by australopiths and early *Homo* (SOM Fig. S2).

At the head location sampling the inferolateral portion of the vertical bundle (hVOI) investigated in this study, all five *Pa. robustus* specimens show a degree of trabecular anisotropy distinct from the isotropic organization of chimpanzee. This supports our second prediction. It is also in accordance with the results provided by Ryan et al. (2018) indicating a more humanlike anisotropic trabecular structure (higher DA values) in australopiths, as compared to the extant nonhuman catarrhine pattern—interpreted as a reduced range of motion of the hip-joint in australopiths, compatible with a fully engaged bipedal gait (Ryan et al., 2018). Interestingly, for this parameter our results also show the intermediate condition for *Gorilla*, which is anyhow expected because gorillas commonly display less variability in joint positioning during locomotion, as compared to *Pan*, probably due to their reduced arboreality and/or larger body size (Remis, 1999; Isler, 2005; Finestone et al., 2018; Georgiou et al., 2019, 2020).

Compared to the extant human condition, a denser trabecular network at most postcranial skeletal sites, including the femoral head, can be considered a plesiomorphic feature shared by all extinct hominins investigated so far (e.g., Macchiarelli et al., 1999; DeSilva and Devlin, 2012; Barak et al., 2013a; Su et al., 2013; Chirchir et al., 2015; Skinner et al., 2015; Zeininger et al., 2016; Su and Carlson, 2017; Cazenave et al., 2019b; but see Kivell et al., 2018, for the proximal humerus). However, for BV/TV assessed at the hVOI, in contrast to our expectation, our results differ slightly from those of Ryan et al. (2018). In our study, *Pa. robustus* is intermediate between the extant human and the African ape conditions. *Paranthropus robustus* is even less distant from the extant human values when compared to (relatively high) values typically shown by *Pan* and *Gorilla* (e.g., Ryan et al., 2018; Tsegai et al., 2018a; Georgiou et al., 2019). Such discrepancies might relate to the different location of the investigated VOIs. Indeed, while our hVOI

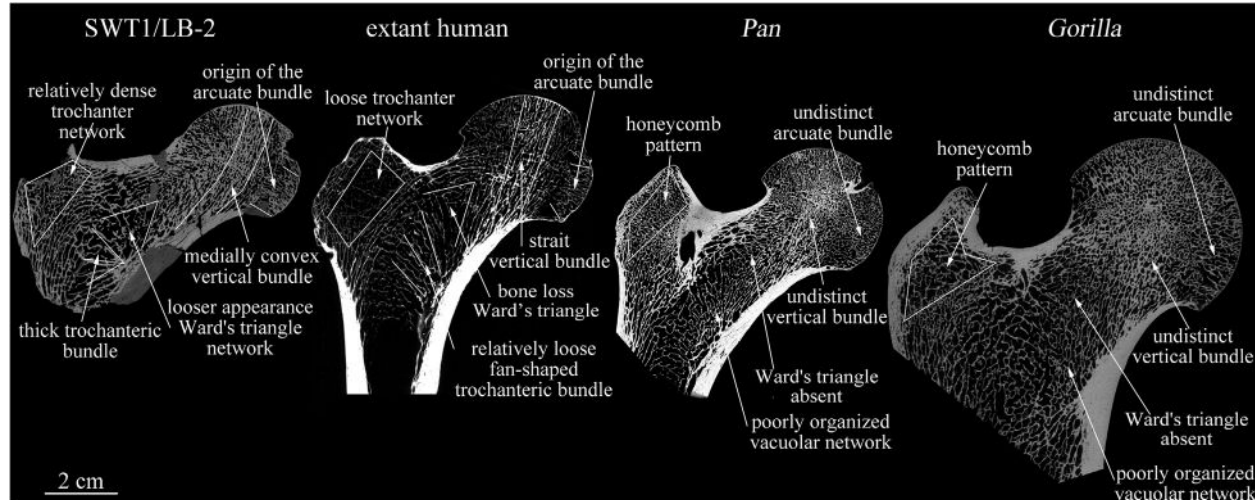


Figure 6. μ XCT-based virtual coronal sections through the femoral head center showing the pattern of the different trabecular structures of the *Paranthropus robustus* proximal femur from Swartkrans (SWT1/LB-2) compared to an extant human, a *Pan troglodytes* and a *Gorilla gorilla* representative.

is extracted within the vertical bundle, the region investigated by Ryan et al. (2018) is by definition denser as it lies at the intersection between the vertical and the arcuate bundles. Nonetheless, what matters here is the unambiguous evidence that the polarity of the structural signals extracted from the center of the femoral head (Ryan et al., 2018), and the hVOI used in this study overlap.

Another result from the study of Ryan et al. (2018) is that both BV/TV and DA assessed at the center of the femoral head do not distinguish *A. africanus* from *Pa. robustus*. However, more recently Georgiou et al. (2020) conducted a comparative analysis of the previously unexplored whole trabecular bone distribution pattern of the femoral head in two fossil hominin specimens from the Sterkfontein Caves: StW 522, representing *A. africanus*, and StW 311, attributed to either early *Homo* or *Pa. robustus*. Along the superior aspect of the head, they found that StW 522 exhibits one high BV/TV concentration in the area located medially and close to the fovea capitis that extends internally as a single pillar. This typically human pattern is distinct from that revealed by StW 311, where a twofold subchondral concentration of high BV/TV, which closely resembles the nonhuman apelike pattern (presumably reflecting a flexed hip posture), extends internally towards the neck (Georgiou et al., 2020: Fig. 4). While needing support from other australopith femora documenting the intraspecific variation range of such structural patterns, these intriguing results point to possible behavioral/locomotor differences between *Australopithecus* and later hominins (likely including *Pa. robustus*) in South Africa, and contribute to the increasing evidence of locomotor diversity within the hominin clade (e.g., Stern, 2000; Ward, 2002, 2013; Ruff, 2008, 2009; DeSilva, 2009; Lovejoy et al., 2009; Zipfel et al., 2011; Haile-Selassie et al., 2012; Green and Alemseged, 2012; Churchill et al., 2013; Marchi, 2015; Kappelman et al., 2016; Ruff et al., 2016; Rein et al., 2017; Kivell et al., 2018).

Because of current technical limitations, we could not test whether the *Pa. robustus* specimens of our sample show a single or twofold subchondral concentration of high BV/TV values along the superior aspect of the femoral head. However, we performed a test using the best-preserved *Pa. robustus* specimen included in our record, SWT1/LB-2. In this fossil we assessed BV/TV in a lateral (α VOI) and a medial (β VOI) cubic VOI (both of 4.2 mm/side, i.e., 12% of the mediolateral head diameter; SOM Fig. S3). The VOIs were approximately placed in correspondence to the two subchondral regions identified by Georgiou et al. (2020: Fig. 2). The β VOI was

positioned at the center of the anteroposterior diameter in the upper region of the vertical bundle, and the α VOI at the same anteroposterior and superoinferior level of the β VOI at the most lateral region of the head (SOM Fig. S3). For comparison, we also performed the same analysis on corresponding VOIs of scaled size identified in one randomly selected human, one chimpanzee, and one gorilla. According to this test (SOM Table S2), the modest BV/TV difference in SWT1/LB-2 between the lateral (53.5%) and the medial spots (59.1%) is compatible with a twofold concentration pattern such as that found in StW 311 (Georgiou et al., 2020).

Despite some technical limitations related to differences in spatial resolution among the microtomographic data of the fossil specimens used in this study, a different picture from the structural signals of the femoral head is provided by the nVOI sampling the vertical bundle at the inferior mid-neck. In this case, contrary to our third expectation, the DA places *Pa. robustus* closer to *Pan*, while, as expected, the BV/TV does not distinguish it from either humans or the African apes. The absolutely small bone volume sampled by the nVOI could partially explain such lower structural heterogeneity, but we note that a proportionally modest sensitivity to load variation of the femoral neck trabecular architecture has been predicted, or measured, in a number of anthropoids, including humans (e.g., Carter et al., 1989; Lotz et al., 1995; Lovejoy et al., 2002; Fajardo et al., 2007; Skedros and Baucom, 2007; Sinclair et al., 2013). Indeed, Fajardo et al. (2007) found strong similarities in trabecular architecture of the inferior and superior regions of the femoral neck of six non-human anthropoids across body size, phylogenetic background, and locomotor mode. It has also been suggested that the trabecular organization of the femoral neck in humans and chimpanzees more likely reflects predominantly shear stresses, which are better accommodated by nonorthogonal asymmetric trabecular tracts (Skedros and Baucon, 2007). While Fajardo et al. (2007) suggested that the similarities in trabecular network organization relate to greater similarity in anthropoid hip joint loading mechanics than previously considered, it is reasonable to assume that, compared to the head compartment where loads are mostly absorbed and transferred by the trabecular network, at the neck compartment it is the cortex that carries most of the loads. Indeed, in humans cortical bone is estimated to carry from ca. 50% to ca. 96% of the loads at the mid-neck and base of the neck, respectively, i.e., considerably more than the thin subcapital cortical shell (ca. 20%; Lotz et al., 1995). Further comparative analyses in extant

hominids and extinct hominins should be performed across the vertical bundle of the neck to assess where the trabecular signal starts to lose heterogeneity. It is anyway noteworthy that, contrary to the results provided by the hVOI, the standard deviations of BV/TV and DA of the nVOI calculated for the extant human sample are higher than those found in our African ape samples. This could result from the larger size of the human sample, but also from its diverse composition (Table 1).

For its trabecular microarrangement, the third compartment of the proximal femur (the trochanteric region) remains quantitatively unexplored in extinct hominins and also poorly assessed in extant humans. It is possible, as future research should test, that this compartment is sensitive to the relative development and action of the hip abductor muscles. For instance, it has been shown in humans that the structure of the trochanteric region (including the 'secondary tensile group' and the 'secondary compressive group' originating in the lateral and medial cortices of the femoral shaft) is determined by and are different from the 'load cases' of the femoral neck (Miller et al., 2002). The trochanteric region can therefore provide complementary information. Also, for reliably modeling the habitual load patterns at the hip joint, as a whole, and at each morphological compartment of the proximal femur, other factors than trabecular bone arrangement should be considered. These of course include the role exerted by the load-sharing cortical bone (e.g., Ohman et al., 1997; Lovejoy et al., 2002; Ruff and Higgins, 2013; Ruff et al., 2016; Cazenave et al., 2019a), but also those played by other stress-carrying elements, such as ligaments and tendons (Lovejoy et al., 2002; Sinclair et al., 2013), which is anyhow a very difficult task when handling fossil specimens.

The influence of body size and sex on trabecular patterning is still under investigation. Some studies indicate that trabecular bone volume fraction tends to vary independently from body size (e.g., Doube et al., 2011; Fajardo et al., 2013; Barak et al., 2013b), while the analysis of a sample of humeri and femora from 34 primate taxa showed a very slight positive allometry (Ryan and Shaw, 2013). With regard to the influence of sex, for BV/TV extant humans show a modest to no degree of sexual dimorphism at the proximal femur (e.g., Chirchir et al., 2015, 2017; Saers et al., 2016; Doershuk et al., 2019). This is supported by our results (SOM Fig. S4) and corroborated by the signal from other skeletal sites (e.g., Chirchir et al., 2015; Saers et al., 2016; but see Scherf et al., 2013, for the proximal humerus). Research performed on *Pan* also provided similar evidence (Scherf et al., 2013; Tsegai et al., 2018a, b). However, the results from the limited sample of gorillas used in this study ($n = 10$) show a different picture. Indeed, at both the head and neck locations, the males systematically show higher BV/TV values than the females (SOM Fig. S4).

If relative size is assumed as a reliable sex indicator for the *Paranthropus* individuals represented in our sample (see Susman et al., 2001; Pickering et al., 2012; Ruff et al., 2018), all larger, more likely male specimens (SK 82, 97 and SWT1/LB-2), show a higher BV/TV at the femoral head than measured in the two smaller, more likely female individuals (SK 3121 and SKW 19). In our study, this pattern is also found at the femoral neck, where SK 97 and SWT1/LB-2 (no data for SK 82) again show higher values than SK 3121 (no data for SKW 19). Combined with the evidence of a certain degree of sexual dimorphism in trabecular bone properties revealed by our *Gorilla* sample, these results possibly corroborate the suggestion of a gorilla-like bimaturism growth pattern in *Pa. robustus* (Lockwood et al., 2007; see also Susman et al., 2001), with a higher bone volume fraction in male *Pa. robustus* than in females, which might relate to behavioural differences between sexes and/or sex-related systemic differences. However, the same picture is not provided by Ryan et al. (2018) for the BV/TV measured at the femoral head center, where the average value of the two

more likely females, SK 3121 and SKW 19 (0.53%) even slightly exceeds that of two more likely males, SK 82 and 97 (0.52%), the lowest BV/TV having been measured in SK 97 (Ryan et al., 2018: Table 2). Given that differences in BV/TV between the forelimb and hindlimb in apes do not clearly reflect differences in locomotor loading (Tsegai et al., 2018a), additional studies on trabecular bone volume fraction systemic patterns are needed for *Paranthropus* to provide further information in the perspective of clarifying and better understanding the possible sex-related variation.

5. Conclusions

The investigation of the trabecular architecture of the proximal femur performed on the assemblage of five variably preserved *Pa. robustus* specimens from the Early Pleistocene South African cave deposits of Swartkrans has revealed a structurally heterogeneous humanlike organization of the network within the three major compartments of this skeletal site (head, neck, greater trochanter). This pattern clearly differs from the typical condition of the extant great apes. In many details, the functionally related trabecular structures forming the medial principal compressive, the lateral principal tensile, and the lateral secondary compressive homologous trabecular systems (Levangie and Norkin, 2005; Kapandji, 2011) closely resemble the extant human condition, but also display some specificities in textural arrangement unreported, or uncommon, in humans and African apes (e.g., a variably marked medially convex vertical bundle, an origin of the arcuate bundle confined to the head portion below the fovea capitis, a looser appearance of the network in the so-called 'Ward's triangle', a greater trochanter trabecular infill of intermediate textural organization and density between the human and the African ape patterns). This adds to the evidence from other studies of actual differences in gait kinematics and locomotor performance between australopiths and extant humans reflecting differences in relative muscular positioning and functioning at the hip joint, i.e., a distinct loading environment (Ruff and Higgins, 2013; Ruff et al., 2016; Cazenave et al., 2019a; Georgiou et al., 2020). However, similarly to the extant hominid pattern revealed by the comparative samples used in this study, the trabecular network properties of the so-called vertical bundle locally assessed at the inferolateral portion of the femoral head—which, as also observed at the center of the head (Ryan et al., 2018), show a humanlike anisotropy but a higher bone volume fraction—differ from the site-specific structural signature of the portion of this bundle closer to the inferior margin of the neck, where the loads are mostly absorbed by the cortical bone (Lotz et al., 1995).

Future comparative research on the australopith proximal femur should focus more carefully on the endostructural organization of the trochanteric region, so far, the least investigated compartment. Indeed, Miller et al. (2002), who simulated trabecular orientation in a 2D finite element model of a human proximal femur subject to various loading directions, concluded that the 'secondary tensile group' and 'secondary compressive group', originating in the lateral and medial cortices of the femoral shaft, are determined by different load cases than in the femoral neck (Miller et al., 2002). In addition, the possible covariation between medial-to-lateral thickening in cortical bone across the neck (Cazenave et al., 2019a) and possible differences in trabecular network properties across the principal tensile structure, i.e., the arcuate bundle, still need to be more carefully investigated. It remains nonetheless to be ascertained if, and to what extent, *Paranthropus* and *Australopithecus* differ in all such endostructural features (Georgiou et al., 2020).

Declaration of competing interest

The authors declare that they have no known competing financial interests or personal relationships that could have appeared to influence the work reported in this paper.

Acknowledgements

For access to fossil and comparative materials, we are grateful to the curatorial staff of the Ditsong National Museum of Natural History, Pretoria; the Evolutionary Studies Institute and the R.A. Dart Collection at the University of the Witwatersrand, Johannesburg; the McGregor Museum of Kimberley; the Museum national d'Histoire naturelle (MNHN), Paris; the Pretoria Bone Collection at the Department of Anatomy of the University of Pretoria; I. Livne (Birchington-on-Sea) for access to the gorilla sample of the Powell-Cotton Museum and M. Skinner (Canterbury) and T. Kivell (Canterbury) for sharing the μ XCT data; and M. Nakamura (Kyoto) and Y. Shintaku (Inuyama) for permission to access Mahale chimpanzee collection. For the extant human comparative sample, ethical clearance was obtained from the Faculty of Health Sciences Research Ethics committee of the University of Pretoria (ref. no. 39/2016). We especially acknowledge B. Billing (Johannesburg), L. Kgasi (Pretoria), D. Morris (Kimberley), S. Potze (Pretoria), M. Tawane (Pretoria) and B. Zipfel (Johannesburg). For the scanning procedure of the *Pan* sample from the MNHN (UMR 7194 CNRS 2018–2020 grants to R.M.) we thank the staff and especially M. Bellato from the AST-RX, plateau d'Accès Scientifique à la Tomographie à Rayons X du MNHN, UMS 2700 2AD CNRS-MNHN, Paris. We thank L. Bam (Pelindaba), K. Jakata (Johannesburg), and R. Kono (Yokohama) for μ XCT scanning at Necsa, Wits, and Tokyo, respectively. Acquisitions at the ESRF were performed by R.M. within the EC TNT project in collaboration with A. Mazurier (Poitiers). For scientific collaboration and availability to run independent measures for interobserver error assessment, we thank A. Beaudet (Johannesburg), A. Mazurier and C. Zanolli (Bordeaux). For discussion, we thank A. Beaudet, J. Braga (Toulouse), L. Bruxelles (Johannesburg and Toulouse), K. Carlson (Johannesburg and Los Angeles), R.J. Clarke (Johannesburg), J. Dumoncel (Toulouse), C. Dunmore (Canterbury), F.E. Grine (Stony Brook), T. Kivell, D. Marchi (Pisa), E. Pouydebat (Paris), M. Skinner, C. Theye (Pretoria), C. Zanolli and B. Zipfel. Finally, we are grateful to David Alba, the Associate Editor, and to three anonymous reviewers for constructive critique that considerably improved this manuscript. We acknowledge the DST-NRF for financial support (Grant # UID23456) to establish the MIXRAD microfocus X-ray tomography facility at Necsa. M.C. was funded by the European Commission (EACEA), Erasmus Mundus programme, AESOP and AESOP + consortia co-ordinated by J. Braga, by the Erasmus Mundus programme, Bakeng se Afrika and by the Fyssen Foundation.

Supplementary Online Material

Supplementary Online Material to this article can be found online at <https://doi.org/10.1016/j.jhevol.2021.102964>.

References

- Aiello, L., Dean, C., 1990. An Introduction to Human Evolutionary Anatomy. Academic Press, New York.
- Balter, V., Blichert-Toft, J., Braga, J., Telouk, P., Thackeray, F., Albarède, F., 2008. U-Pb dating of fossil enamel from the Swartkrans Pleistocene hominid site, South Africa. *Earth Planet Sci. Lett.* 267, 236–246.
- Barak, M.M., Lieberman, D.E., Hublin, J.-J., 2011. A Wolff in sheep's clothing: Trabecular bone adaptation in response to changes in joint loading orientation. *Bone* 49, 1141–1151.
- Barak, M.M., Lieberman, D.E., Raichlen, D., Pontzer, H., Warrener, A.G., Hublin, J.-J., 2013a. Trabecular evidence for a human-like gait in *Australopithecus africanus*. *PLoS One* 8, e77687.
- Barak, M.M., Lieberman, D.E., Hublin, J.-J., 2013b. Of mice, rats and men: Trabecular bone architecture in mammals scales to body mass with negative allometry. *J. Struct. Biol.* 183, 123–131.
- Beaupré, G.S., Orr, T.E., Carter, D.R., 1990. An approach for time-dependent bone modeling and remodeling—theoretical development. *J. Orthop. Res.* 8, 651–661.
- Biewener, A.A., Fazzalari, N.L., Konieczynski, D.D., Baudinette, R.V., 1996. Adaptive changes in trabecular architecture in relation to functional strain patterns and disuse. *Bone* 19, 1–8.
- Bishop, P.J., Clemente, C.J., Hocknull, S.A., Barrett, R.S., Lloyd, D.G., 2017. The effects of cracks on the quantification of the cancellous bone fabric tensor in fossil and archaeological specimens: A simulation study. *J. Anat.* 230, 461–470.
- Bonewald, L.F., Johnson, M.L., 2008. Osteocytes, mechanosensing and Wnt signaling. *Bone* 42, 606–615.
- Brain, C.K., 1981. The Hunters or the Hunted? An Introduction to African Cave Taphonomy. The University of Chicago Press, Chicago.
- Carlson, K.J., Judex, S., 2007. Increased non-linear locomotion alters diaphyseal bone shape. *J. Exp. Biol.* 210, 3117–3125.
- Carter, D.R., Orr, T.E., Fyhrie, D.P., 1989. Relationships between loading history and femoral cancellous bone architecture. *J. Biomech.* 22, 231–244.
- Cazenave, M., 2015. The inner structural morphology of the femoral head of *Paranthropus robustus*. Master Thesis, Université Toulouse III – Paul Sabatier.
- Cazenave, M., 2018a. Caractérisation multi-site de la distribution osseuse corticale et de l'organisation du réseau trabéculaire du squelette postcrânien de *Paranthropus robustus*: implications taxonomiques, fonctionnelles et paléobiologiques. Ph.D. Dissertation, Université Toulouse III – Paul Sabatier.
- Cazenave, M., 2018b. Caractéristiques endostructurales du squelette postcrânien de *Paranthropus robustus*. Implications taxinomiques, fonctionnelles et paléobiologiques. *Bull. Mem. Soc. Anthropol. Paris* 30, S13.
- Cazenave, M., Braga, J., de Beer, F., Hoffman, J.W., Macchiarelli, R., Thackeray, J.F., 2015. The inner structural morphology of the femoral head of *Paranthropus robustus*. *Proc. Eur. Soc. Stud. Hum. Evol.* 5, 68.
- Cazenave, M., Braga, J., Oettlé, A., Pickering, T.R., Heaton, J.L., Nakatsukasa, M., Thackeray, J.F., de Beer, F., Hoffman, J., Dumoncel, J., Macchiarelli, R., 2019a. Cortical bone distribution in the femoral neck of *Paranthropus robustus*. *J. Hum. Evol.* 135, 10266.
- Cazenave, M., Oettlé, A., Pickering, T.R., Heaton, J.L., Nakatsukasa, M., de Beer, F., Hoffman, J., Macchiarelli, R., 2019b. The SKX 1084 hominin patella from Swartkrans Member 2, South Africa: An integrated analysis of its outer morphology and inner structure. *C. R. Palevol* 18, 223–235.
- Cazenave, M., Oettlé, A., Pickering, T.R., Heaton, J.L., Nakatsukasa, M., Thackeray, J.F., de Beer, F., Hoffman, J., Macchiarelli, R., 2020. Trabecular organization of the proximal femur in *Paranthropus robustus*: Implications for the assessment of its hip joint loading conditions. Kent Data Repository. <https://doi.org/10.22024/Unikent/01.01.115.6>.
- Chang, G., Pakin, S.K., Schweitzer, M.E., Saha, P.K., Regatte, R.R., 2008. Adaptations in trabecular bone microarchitecture in Olympic athletes determined by 7T MRI. *J. Magn. Reson. Imag.* 27, 1089–1095.
- Chirchir, H., Kivell, T.L., Ruff, C.B., Hublin, J.-J., Carlson, K.J., Zipfel, B., Richmond, B.G., 2015. Recent origin of low trabecular bone density in modern humans. *Proceedings of the National Academy of Sciences USA* 112, 366–371.
- Chirchir, H., Zeininger, A., Nakatsukasa, M., Ketcham, R.A., Richmond, B.G., 2017. Does trabecular bone structure within the metacarpal heads of primates vary with hand posture? In: Macchiarelli, R., Zanolli, C. (Eds.), *Hominin Biomechanics, Virtual Anatomy and Inner Structural Morphology: From Head to Toe. A Tribute to Laurent Puymerail*. Comptes Rendus Palevol, vol. 16, pp. 533–544.
- Churchill, S.E., Holliday, T.W., Carlson, K.J., Jashashvili, T., Macias, M.E., Mathews, S., Sparling, T.L., Schmid, P., de Ruiter, D.J., Berger, L.R., 2013. The upper limb of *Australopithecus sediba*. *Science* 340, 1233477.
- Claxton, A., 2018. A re-assessment of femoral neck cortical thickness. Ph.D. Dissertation, Boston University.
- Correnti, V., 1955. Le basi morfomeccaniche della struttura dell'osso iliaco. *Riv. Antropol.* 42, 289–336.
- Crabtree, N., Loveridge, N., Parker, M., Rushton, N., Power, J., Bell, K.L., Beck, T.J., Reeve, J., 2001. Intracapsular hip fracture and the region-specific loss of cortical bone: Analysis by peripheral quantitative computed tomography. *J. Bone Miner. Res.* 16, 1318–1328.
- Cresswell, E.N., Goff, M.G., Nguyen, T.M., Lee, W.X., Hernandez, C.J., 2015. Spatial relationships between bone formation and mechanical stress within cancellous bone. *J. Biomech.* 49, 222–228.
- Crompton, R.H., Sellers, W.I., Thorpe, S.K.S., 2010. Arboreality, terrestriality and bipedalism. *Phil. Trans. Biol. Sci.* 365, 3301–3314.
- Culmann, K., 1866. Die Graphische Statistik. Verlag von Meyer & Zeller, Zürich.
- Cunningham, C.A., Black, S.M., 2009. Anticipating bipedalism: Trabecular organization in the newborn ilium. *J. Anat.* 214, 817–829.
- Curnoe, D., Grün, R., Taylor, L., Thackeray, F., 2001. Direct ESR dating of a Pliocene hominin from Swartkrans. *J. Hum. Evol.* 40, 379–391.
- Dayal, M.R., Kegley, A.D.T., Štrkalj, G., Bidmos, M.A., Kuykendall, K.L., 2009. The history and composition of the Raymond A. Dart collection of human skeletons at the University of the Witwatersrand, Johannesburg, South Africa. *Am. J. Phys. Anthropol.* 140, 324–335.

- Delson, E., 1988. Chronology of South African australopith site units. In: Grine, F.E. (Ed.), *Evolutionary History of the "Robust" Australopithecines*. Aldine de Gruyter, New York, pp. 317–324.
- Demissie, S., Dupuis, J., Cupples, L.A., Beck, T., Kiel, D.P., Karasik, D., 2007. Proximal hip geometry is linked to several chromosomal regions: Genome-wide linkage results from the Framingham Osteoporosis Study. *Bone* 40, 743–750.
- DeSilva, J.M., 2009. Functional morphology of the ankle and the likelihood of climbing in early hominins. *Proc. Natl. Acad. Sci. USA* 106, 6567–6572.
- DeSilva, J.M., Devlin, M.J., 2012. A comparative study of the trabecular bony architecture of the talus in humans, non-human primates, and *Australopithecus*. *J. Hum. Evol.* 63, 536–551.
- Doershuk, L.J., Saers, J.P., Shaw, C.N., Jashashvili, T., Carlson, K.J., Stock, J.T., Ryan, T.M., 2019. Complex variation of trabecular bone structure in the proximal humerus and femur of five modern human populations. *Am. J. Phys. Anthropol.* 168, 104–118.
- Doran, D.M., 1993a. Comparative locomotor behavior of chimpanzees and bonobos: the influence of morphology on locomotion. *Am. J. Phys. Anthropol.* 91, 83–98.
- Doran, D.M., 1993b. Sex differences in adult chimpanzee positional behavior: the influence of body size on locomotion and posture. *Am. J. Phys. Anthropol.* 91, 99–115.
- Doran, D.M., 1997. Ontogeny of locomotion in mountain gorillas and chimpanzees. *J. Hum. Evol.* 32, 323–344.
- Doube, M., Kłosowski, M.M., Wiktorowicz-Conroy, A.M., Hutchinson, J.R., Shefelbine, S.J., 2011. Trabecular bone scales allometrically in mammals and birds. *Proc. R. Soc. B* 278, 3067–3073.
- Estrada, K., Styrkarsdottir, U., Evangelou, E., Hsu, Y.H., Duncan, E.L., Ntzani, E.E., Oei, L., Albagha, O.M., Amin, N., Kemp, J.P., Koller, D.L., Li, G., Liu, C.T., Minster, R.L., Moayyeri, A., Vandeput, L., Willner, D., Xiao, S.M., Yerges-Armstrong, L.M., Zheng, H.F., Alonso, N., Eriksson, J., Kammerer, C.M., Kaptope, S.K., Leo, P.J., Thörleifsson, G., Wilson, S.G., Wilson, J.F., Aalto, V., Alen, M., Aragaki, A.K., Aspelund, T., Center, J.R., Dailiana, Z., Duggan, D.J., Garcia, M., Garcia-Giralt, N., Giroux, S., Hallmans, G., Hocking, L.J., Husted, L.B., Jameson, K.A., Khusainova, R., Kim, G.S., Kooperberg, C., Koromila, T., Kruk, M., Laaksonen, M., Lacroix, A.Z., Lee, S.H., Leung, P.C., Lewis, J.R., Masi, L., Mencej-Bedrac, S., Nguyen, T.V., Nogues, X., Patel, M.S., Prezelj, J., Rose, L.M., Scollen, S., Siggeirsdottrí, K., Smith, A.V., Svensson, O., Trompet, S., Trummer, O., van Schoor, N.M., Woo, J., Zhu, K., Balcells, S., Brandi, M.L., Buckley, B.M., Cheng, S., Christiansen, C., Cooper, C., Dedousis, G., Ford, I., Frost, M., Goltzman, D., Gonzalez-Macias, J., Kahonen, M., Karlsson, M., Khusnudinova, E., Koh, J.M., Kollia, P., Langdahl, B.L., Leslie, W.D., Lips, P., Ljunggren, O., Lorenc, R.S., Marc, J., Mellstrom, D., Obermayer-Pietsch, B., Olmos, J.M., Pettersson-Kymmer, U., Reid, D.M., Riancho, J.A., Ridker, P.M., Rousseau, F., Slagboom, P.E., Tang, N.L., Urreizti, R., Van Hul, W., Viikari, J., Zarzabeitia, M.T., Aulchenko, Y.S., Grundberg, E., Herrera, L., Ingvarsson, T., Johannsdottir, H., Kwan, T., Li, R., Luben, R., Medina-Gomez, C., Palsson, S.T., Reppe, S., Rotter, J.I., Sigurdsson, G., van Meurs, J.B., Verlaan, D., Williams, F.M., Wood, A.R., Zhou, Y., Gautvik, K.M., Pastinen, T., Raychaudhuri, S., Cauley, J.A., Chasman, D.I., Clark, G.R., Cummings, S.R., Danoy, P., Dennison, E.M., Eastell, R., Eisman, J.A., Gudnason, V., Hofman, A., Jackson, R.D., Jones, G., Jukema, J.W., Khaw, K.T., Lehtimaki, T., Liu, Y., Lorentzon, M., McCloskey, E., Mitchell, B.D., Nandakumar, K., Nicholson, G.C., Oostra, B.A., Peacock, M., Pols, H.A., Prince, R.L., Raitakari, O., Reid, I.R., Robbins, J., Sambrook, P.N., Sham, P.C., Shuldiner, A.R., Tylavsky, F.A., van Duijn, C.M., Wareham, N.J., Cupples, L.A., Econs, M.J., Evans, D.M., Harris, T.B., Kung, A.W., Psaty, B.M., Reeve, J., Spector, T.D., Streeten, E.A., Zillikens, M.C., Thorsteinsdóttir, U., Ohlsson, C., Karasik, D., Richards, J.B., Brown, M.A., Stefansson, K., Uitterlinden, A.G., Ralston, S.H., Ioannidis, J.P., Kiel, D.P., Rivadeneira, F., 2012. Genome-wide meta-analysis identifies 56 bone mineral density loci and reveals 14 loci associated with risk of fracture. *Nat. Genet.* 44, 491–501.
- Fajardo, R.J., Müller, R., 2001. Three-dimensional analysis of nonhuman primate trabecular architecture using micro-computed tomography. *Am. J. Phys. Anthropol.* 115, 327–336.
- Fajardo, R.J., Ryan, T.M., Kappelman, J., 2002. Assessing the accuracy of high-resolution X-ray computed tomography of primate trabecular bone by comparisons with histological sections. *Am. J. Phys. Anthropol.* 118, 1–10.
- Fajardo, R.J., Müller, R., Ketcham, R.A., Colbert, M., 2007. Nonhuman anthropoid primate femoral neck trabecular architecture and its relationship to locomotor mode. *Anat. Rec.* 290, 422–436.
- Fajardo, R.J., Desilva, J.M., Manoharan, R.K., 2013. Lumbar vertebral body bone microstructural scaling in small to medium-sized strepsirrhines. *Anat. Rec.* 296, 210–226.
- Finestone, E.M., Brown, M.H., Ross, S.R., Pontzer, H., 2018. Great ape walking kinematics: Implications for hominoid evolution. *Am. J. Phys. Anthropol.* 166, 43–55.
- Friedl, L., Claxton, A.G., Walker, C.S., Churchill, S.E., Holliday, T.W., Hawks, J., Marchi, D., 2019. Femoral neck and shaft structure in *Homo naledi* from the Dinaledi Chamber (Rising Star System, South Africa). *J. Hum. Evol.* 133, 61–77.
- Georgiou, L., Kivell, T.L., Pahr, D.H., Buck, L.T., Skinner, M.M., 2019. Trabecular architecture of the great ape and human femoral head. *J. Anat.* 234, 679–693.
- Georgiou, L., Dunmore, C.J., Bardo, A., Buck, L.T., Hublin, J.-J., Pahr, D.H., Stratford, D., Synek, A., Kivell, T.L., Skinner, M.M., 2020. Evidence for habitual climbing in a middle Pleistocene hominin in South Africa. *Proc. Natl. Acad. Sci. USA* 117, 8416–8423.
- Gibbon, R.J., Rayne, T., Sutton, M.B., Heaton, J.L., Kuman, K., Clarke, R.J., Brain, C.K., Granger, D.E., 2014. Quaternary geochronology cosmogenic nuclide burial dating of hominin-bearing Pleistocene cave deposits at Swartkrans, South Africa. *Quat. Geochronol.* 24, 10–15.
- Green, D.J., Alemseged, Z., 2012. *Australopithecus afarensis* scapular ontogeny, function, and the role of climbing in human evolution. *Science* 338, 514–517.
- Gross, T., Kivell, T.L., Skinner, M.M., Huynh Nguyen, N., Pahr, D.H., 2014. A CT-image-based framework for the holistic analysis of cortical and trabecular bone morphology. *Paleontol. Electron.* 17, 33A.
- Guldborg, R.E., Caldwell, N.J., Guo, X.E., 1997. Mechanical stimulation of tissue repair in the hydraulic bone chamber. *J. Bone Miner. Res.* 12, 1295–1302.
- Haile-Selassie, Y., Saylor, B., Deino, A., Levin, N., Alene, M., Latimer, B., 2012. A new hominin foot from Ethiopia shows multiple Pliocene bipedal adaptations. *Nature* 483, 565–569.
- Havill, L.M., Mahaney, M.C., Binkley, T.L., Specker, B.L., 2007. Effects of genes, sex, age, and activity on BMC, bone size, and areal and volumetric BMD. *J. Bone Miner. Res.* 22, 737–746.
- Havill, L.M., Allen, M.R., Bredbenner, T.L., Burr, D.B., Nicolella, D.P., Turner, C.H., Warren, D.M., Mahaney, M.C., 2010. Heritability of lumbar trabecular bone mechanical properties in baboons. *Bone* 46, 835–840.
- Herries, A.R., Curnoe, D., Adams, J.W., 2009. A multi-disciplinary seriation of early *Homo* and *Paranthropus* bearing palaeocaves in Southern Africa. *Quat. Int.* 202, 14–28.
- Hou, R., Cole, S.A., Graff, M., Haack, K., Laston, S., Comuzzie, A.G., Mehta, N.R., Ryan, K., Cousminer, D.L., Zemel, B.S., Grant, S.F.A., Mitchell, B.D., Shypailo, R.J., Gourlay, M.L., North, K.E., Butte, N.F., Grant, S.F., 2020. Genetic variants affecting bone mineral density and bone mineral content at multiple skeletal sites in Hispanic children. *Bone* 132, 11517.
- Hunt, K.D., 1991. Positional behavior in the Hominoidea. *Int. J. Primatol.* 12, 95–118.
- Isler, K., 2005. 3D-Kinematics of vertical climbing in hominoids. *Am. J. Phys. Anthropol.* 126, 66–81.
- Jang, I.G., Kim, I.Y., 2008. Computational study of Wolff's law with trabecular architecture in the human proximal femur using topology optimization. *J. Biomech.* 41, 2353–2361.
- Jude, S., Garman, R., Squire, M., Leah-Rae, D., Rubin, C., 2004. Genetically based influences on the site-specific regulation of trabecular and cortical bone morphology. *J. Bone Miner. Res.* 19, 600–606.
- Kapandji, A.I., 2011. *The Physiology of the Joints. Vol. 2. The Lower Limb*, 6th ed. Elsevier, Edinburgh.
- Kappelman, J., Ketcham, R.A., Pearce, S., Todd, L., Akins, W., Colbert, M.W., Feseha, M., Maisano, J.A., Witzel, A., 2016. Perimortem fractures in Lucy suggest mortality from fall out of tall tree. *Nature* 537, 503–507.
- Ketcham, R.A., Ryan, T.M., 2004. Quantification and visualization of anisotropy in trabecular bone. *J. Microsc.* 213, 158–171.
- Kivell, T.L., Skinner, M.M., Lazenby, R., Hublin, J.-J., 2011. Methodological considerations for analyzing trabecular architecture: An example from the primate hand. *J. Anat.* 218, 209–225.
- Kivell, T.L., 2016. A review of trabecular bone functional adaptation: What have we learned from trabecular analyses in extant hominoids and what can we apply to fossils? *J. Anat.* 228, 569–594.
- Kivell, T.L., Davenport, R., Hublin, J.-J., Thackeray, J.F., Skinner, M.M., 2018. Trabecular architecture and joint loading of the proximal humerus in extant hominoids, *Atelles*, and *Australopithecus africanus*. *Am. J. Phys. Anthropol.* 167, 348–365.
- Kozma, E.E., Webb, N.M., Harcourt-Smith, W.E.H., Raichlen, D.A., D'Août, K., Brown, M.H., Finestone, E.M., Ross, S.R., Aerts, P., Pontzer, H., 2018. Hip extensor mechanics and the evolution of walking and climbing capabilities in humans, apes, and fossil hominins. *Proc. Natl. Acad. Sci. USA* 115, 4134–4139.
- L'Abbé, E.N., Loots, M., Meiring, J.H., 2005. The Pretoria Bone Collection: A modern South African skeletal sample. *Homo* 56, 197–205.
- Lanyon, L.E., 1973. Analysis of surface bone strain in the sheep during normal locomotion. *J. Biomed.* 6, 41–49.
- Lazenby, R.A., Skinner, M.M., Kivell, T.L., Hublin, J.-J., 2011. Scaling VOI size in 3D ICT studies of trabecular bone: A test of the over-sampling hypothesis. *Am. J. Phys. Anthropol.* 144, 196–203.
- Legendre, P., 2018. *lmodel2: Model II Regression*. R package Version 1.7-3. <https://CRAN.R-project.org/package=lmodel2>.
- Levangie, P.K., Norkin, C.C., 2005. *Joint Structure and Function: A Comprehensive Analysis*. F.A. Davis, Philadelphia.
- Lockwood, C.A., Menter, C.G., Moggi-Cecchi, J., Keyser, A.W., 2007. Extended male growth in a fossil hominin species. *Science* 318, 1443–1446.
- Lotz, J.C., Cheal, E.J., Hayes, W.C., 1995. Stress distributions within the proximal femur during gait and falls: Implications for osteoporotic fracture. *Osteoporos. Int.* 5, 252–261.
- Lovejoy, C.O., 1988. Evolution of human walking. *Sci. Am.* 259, 118–125.
- Lovejoy, C.O., 2005. The natural history of human gait and posture. Part 2. Hip and thigh. *Gait Posture* 21, 113–124.
- Lovejoy, C.O., Cohn, M.J., White, T.D., 1999. Morphological analysis of the mammalian postcranium: A developmental perspective. *Proc. Natl. Acad. Sci. USA* 96, 13247–13252.
- Lovejoy, C.O., Meindl, R.S., Ohman, J.C., Heiple, K.G., White, T.D., 2002. The Maka femur and its bearing on the antiquity of human walking: Applying contemporary concepts of morphogenesis to the human fossil record. *Am. J. Phys. Anthropol.* 119, 97–133.
- Lovejoy, C.O., Suwa, G., Spurlock, L., Asfaw, B., White, T., 2009. The pelvis and femur of *Ardipithecus ramidus*: The emergence of upright walking. *Science* 326, 71e1–71e6.

- Macchiarelli, R., Bondioli, L., 2000. Multimedia dissemination of the "Isola Sacra" human paleobiological project: Reconstructing lives, habits, and deaths of the "ancient Roman people" by means of advanced investigative methods. In: Guarino, A. (Ed.), Proceedings of 2nd International Congress on Science and Technology for the Safeguard of Cultural Heritage in the Mediterranean Basin, vol. 2. Elsevier, Paris, pp. 1075–1080.
- Macchiarelli, R., Bondioli, L., Galichon, V., Tobias, P.V., 1999. Hip bone trabecular architecture shows uniquely distinctive locomotor behaviour in South African australopithecines. *J. Hum. Evol.* 36, 211–232.
- Macchiarelli, R., Rook, L., Bondioli, L., 2001. Comparative analysis of the iliac trabecular architecture in extant and fossil primates by means of digital image processing techniques: Implications for the reconstruction of fossil locomotor behaviours. In: de Bonis, L., Koufos, G., Andrews, P. (Eds.), Hominoid Evolution and Climatic Change in Europe, Phylogeny of the Neogene Hominoid Primates of Eurasia, vol. 2. Cambridge University Press, Cambridge, pp. 60–101.
- MacLatchy, L., Müller, R., 2002. A comparison of the femoral head and neck trabecular architecture of *Galago* and *Proterotherium* using micro-computed tomography (microCT). *J. Hum. Evol.* 43, 89–105.
- Maga, M., Kappelman, J., Ryan, T.M., Ketcham, R.A., 2006. Preliminary observations on the calcaneal trabecular microarchitecture of extant large-bodied hominoids. *Am. J. Phys. Anthropol.* 129, 410–417.
- Marchi, D., 2015. Using the morphology of the hominoid distal fibula to interpret arboreality in *Australopithecus afarensis*. *J. Hum. Evol.* 85, 136–148.
- Medina-Gomez, C., Kemp, J.P., Trajanoska, K., Luan, J.A., Chesi, A., Ahluwalia, T.S., Mook-Kanamori, D.O., Ham, A., Hartwig, F.P., Evans, D.S., Joro, R., Nedeljkovic, I., Zheng, H.F., Zhu, K., Atalay, M., Liu, C.T., Nethander, M., Broer, L., Porleifsson, G., Mullin, B.H., Handelman, S.K., Nalls, M.A., Jessen, L.E., Heppe, D.H.M., Richards, J.B., Wang, C., Chawes, B., Schraut, K.E., Amin, N., Wareham, N., Karasik, D., Van der Velde, N., Ikram, M.A., Zemel, B.S., Zhou, Y., Carlson, C.J., Liu, Y., McGuigan, F.E., Boer, C.G., Bonnelykke, K., Ralston, S.H., Robbins, J.A., Zillikens, M.C., Langenberg, C., Li-Gao, R., Williams, F.M.K., Harris, T.B., Akesson, K., Jackson, R.D., Sigurdsson, G., den Heijer, M., van der Eerden, B.C.J., de la Peppel, J., Spector, T.D., Pennell, C., Horta, B.L., Felix, J.F., Zhao, J.H., Wilson, S.G., de Mutsert, R., Bisgaard, H., Styrkársdóttir, U., Jaddoe, V.W., Orwoll, E., Lakka, T.A., Scott, R., Grant, S.F.A., Lorentzon, M., van Duijn, C.M., Wilson, J.F., Stefansson, K., Psaty, B.M., Kiel, D.P., Ohlsson, C., Ntzani, E., van Wijnen, A.J., Forgetta, V., Ghanbari, M., Logan, J.G., Williams, G.R., Bassett, J.H.D., Croucher, P.I., Evangelou, E., Uitterlinden, A.G., Ackert-Bicknell, C.L., Tobias, J.H., Evans, D.M., Rivadeneira, F., 2018. Life-course genome-wide association study meta-analysis of total body BMD and assessment of age-specific effects. *Am. J. Hum. Genet.* 102, 88–102.
- Miller, Z., Fuchs, M.B., Arcan, M., 2002. Trabecular bone adaptation with an orthotropic material model. *J. Biomech.* 35, 247–256.
- Milovanovic, P., Djonic, D., Hahn, M., Amling, M., Busse, B., Djuric, M., 2017. Region-dependent patterns of trabecular bone growth in the human proximal femur: A study of 3D bone microarchitecture from early postnatal to late childhood period. *Am. J. Phys. Anthropol.* 164, 281–291.
- Mittra, E., Rubin, C., Qin, Y.X., 2005. Interrelationship of trabecular mechanical and microstructural properties in sheep trabecular bone. *J. Biomech.* 38, 1229–1237.
- Mori, T., Okimoto, N., Sakai, A., Okazaki, Y., Nakura, N., Notomi, T., Nakamura, T., 2003. Climbing exercise increases bone mass and trabecular bone turnover through transient regulation of marrow osteogenic and osteoclastogenic potentials in mice. *J. Bone Miner. Res.* 18, 2002–2009.
- Morris, A.G., 1984. Osteological analysis of the proto-historic populations of the Northern Cape and Western Orange Free State. Ph.D. Dissertation, University of the Witwatersrand, South Africa.
- Ohman, J.C., 1993. Cross sectional geometric properties from biplanar radiographs and computed tomography: functional application to the humerus and femur in Hominoids. Ph.D. Dissertation, Kent State.
- Ohman, J.C., Krochta, T.J., Lovejoy, C.O., Mensforth, R.P., Latimer, B., 1997. Cortical bone distribution in the femoral neck of hominoids: Implications for the locomotion of *Australopithecus afarensis*. *Am. J. Phys. Anthropol.* 104, 117–131.
- O'Neill, M.C., Dobson, S.D., 2008. The degree and pattern of phylogenetic signal in primate long-bone structure. *J. Hum. Evol.* 54, 309–322.
- Pickering, T.R., Kramers, J.D., Hancox, P.J., de Ruiter, D.J., Woodhead, J.D., 2011. Contemporary flowstone development links early hominin bearing cave deposits in South Africa. *Earth Planet. Sci. Lett.* 306, 23–32.
- Pickering, T.R., Heaton, J.L., Clarke, R.J., Sutton, M.B., Brain, C.K., Kuman, K., 2012. New hominid fossils from Member 1 of the Swartkrans formation, South Africa. *J. Hum. Evol.* 62, 618–628.
- Pickering, R., Herries, A.I., Woodhead, J.D., Hellstrom, J.C., Green, H.E., Paul, B., Ritzman, T., Strait, D.S., Schoville, B.J., Hancox, P.J., 2019. U–Pb-dated flowstones restrict South African early hominin record to dry climate phases. *Nature* 565, 226–229.
- Pina, M., Alba, D.M., Moyà-Solà, S., Almécija, S., 2019. Femoral neck cortical bone distribution of dryopithecine apes and the evolution of hominid locomotion. *J. Hum. Evol.* 136, 102651.
- Polk, J.D., Blumenfeld, J., Ahlumwalia, D., 2008. Knee posture predicted subchondral apparent density in the distal femur: an experimental validation. *Anat. Rec.* 291, 293–302.
- Pontzer, H., Lieberman, D.E., Momin, E., Devlin, M.J., Polk, J.D., Hallgrímsson, B., Cooper, D.M.L., 2006. Trabecular bone in the bird knee responds with high sensitivity to changes in load orientation. *J. Exp. Biol.* 209, 57–65.
- Pontzer, H., Raichlen, D.A., Rodman, P.S., 2014. Bipedal and quadrupedal locomotion in chimpanzees. *J. Hum. Evol.* 66, 64–82.
- R Core Team, 2018. R: A language and environment for statistical computing. R Foundation for Statistical Computing, Vienna. <http://www.R-project.org/>.
- Rafferty, K.L., 1998. Structural design of the femoral neck in primates. *J. Hum. Evol.* 34, 361–383.
- Raichlen, D.A., Gordon, A.D., Foster, A.D., Webber, J.T., Sukhdeo, S.M., Scott, R.S., Gosman, J.H., Ryan, T.M., 2015. An ontogenetic framework linking locomotion and trabecular bone architecture with applications for reconstructing hominin life history. *J. Hum. Evol.* 81, 1–12.
- Rein, T.R., Harrison, T., Carlson, K.J., Harvati, K., 2017. Adaptation to suspensory locomotion in *Australopithecus sediba*. *J. Hum. Evol.* 104, 1–12.
- Reissis, D., Abel, R.L., 2012. Development of fetal trabecular micro-architecture in the humerus and femur. *J. Anat.* 220, 496–503.
- Remis, M., 1995. Effects of body size and social context on arboreal activities of lowland gorillas in the Central African Republic. *Am. J. Phys. Anthropol.* 97, 413–433.
- Remis, M.J., 1999. Tree structure and sex differences in arboreality among western lowland gorillas (*Gorilla gorilla gorilla*) at Bai Hokou, Central African Republic. *Primates* 40, 383–396.
- Robinson, J.T., 1972. Early Hominid Posture and Locomotion. University of Chicago Press, Chicago.
- Ruff, C.B., 2008. Femoral/humeral strength in early African *Homo erectus*. *J. Hum. Evol.* 54, 383–390.
- Ruff, C.B., 2009. Relative limb strength and locomotion in *Homo habilis*. *Am. J. Phys. Anthropol.* 138, 90–100.
- Ruff, C.B., Higgins, R., 2013. Femoral neck structure and function in early hominins. *Am. J. Phys. Anthropol.* 150, 512–525.
- Ruff, C.B., McHenry, H.M., Thackeray, J.F., 1999. Cross-sectional morphology of the SK 82 and 97 proximal femora. *Am. J. Phys. Anthropol.* 109, 509–521.
- Ruff, C.B., Holt, B.H., Trinkaus, E., 2006. Who's afraid of the big bad Wolff?: "Wolff's Law" and bone functional adaptation. *Am. J. Phys. Anthropol.* 129, 484–498.
- Ruff, C.B., Burgess, M.L., Ketcham, R.A., Kappelman, J., 2016. Limb bone structural proportions and locomotor behavior in AL 288-1 ("Lucy"). *PLoS One* 11, e0166095.
- Ruff, C.B., Burgess, M.L., Squyres, N., Junno, J.A., Trinkaus, E., 2018. Lower limb articular scaling and body mass estimation in Pliocene and Pleistocene hominins. *J. Hum. Evol.* 115, 85–111.
- Ruff, B., Higgins, R.W., Carlson, K.J., 2020. Long bone Cross-sectional geometry. In: Bernhard Zipfel, B., Richmond, B.G., Carol, V., Ward, C.V. (Eds.), Hominin Postcranial Remains from Sterkfontein. Oxford University Press, Oxford, South Africa, pp. 308–320.
- Ryan, T.M., Carlson, K.J., Gordon, A.D., Jablonski, N., Shaw, C.N., Stock, J.T., 2018. Human-like hip joint loading in *Australopithecus africanus* and *Paranthropus robustus*. *J. Hum. Evol.* 121, 12–24.
- Ryan, T.M., Ketcham, R., 2002a. The three-dimensional structure of trabecular bone in the femoral head of strepsirrhine primates. *J. Hum. Evol.* 43, 1–26.
- Ryan, T.M., Ketcham, R., 2002b. Femoral head trabecular bone structure in two omomyid primates. *J. Hum. Evol.* 43, 241–263.
- Ryan, T.M., Ketcham, R., 2005. Angular orientation of trabecular bone in the femoral head and its relationship to hip joint loads in leaping primates. *J. Morphol.* 265, 249–263.
- Ryan, T.M., Krovitz, G.E., 2006. Trabecular bone ontogeny in the human proximal femur. *J. Hum. Evol.* 51, 591–602.
- Ryan, T.M., Shaw, C.N., 2012. Unique suites of trabecular bone features characterize locomotor behavior in human and non-human anthropoid primates. *PLoS One* 7, 1–11.
- Ryan, T.M., Shaw, C.N., 2013. Trabecular bone microstructure scales allometrically in the primate humerus and femur. *Proc. R. Soc. B* 280, 20130172.
- Ryan, T.M., Shaw, C.N., 2015. Gracility of the modern *Homo sapiens* skeleton is the result of decreased biomechanical loading. *Proc. Natl. Acad. Sci. USA* 112, 372–377.
- Ryan, T.M., Walker, A., 2010. Trabecular bone structure in the humeral and femoral heads of anthropoid primates. *Anat. Rec.* 293, 719–729.
- Saers, J.P.P., Cazorla-Bak, Y., Shaw, C.N., Stock, J.T., Ryan, T.M., 2016. Trabecular bone structural variation throughout the human lower limb. *J. Hum. Evol.* 97, 97–108.
- Saparin, P., Scherf, H., Hublin, J.-J., Fratzl, P., Weinkamer, R., 2011. Structural adaptation of trabecular bone revealed by position resolved analysis of proximal femora of different primates. *Anat. Rec.* 294, 55–67.
- Scherf, H., Harvati, K., Hublin, J.-J., 2013. A comparison of proximal humeral cancellous bone of great apes and humans. *J. Hum. Evol.* 65, 29–38.
- Schneider, C.A., Rasband, W.S., Eliceiri, K.W., 2012. NIH Image to ImageJ: 25 years of image analysis. *Nat. Methods* 9, 671–675.
- Shaw, C., Ryan, T., 2012. Does skeletal anatomy reflect adaptation to locomotor patterns? Cortical and trabecular architecture in human and nonhuman anthropoids. *Am. J. Phys. Anthropol.* 147, 187–200.
- Shimizu, D., Gunji, H., Hashimoto, H., Hosaka, K., Huffman, M.A., Matsumoto-Oda, A., Kawanaka, K., Nishida, T., 2002. The four chimpanzee skulls collected in the Mahale Mountains, Tanzania. *Anthropol. Sci.* 110, 251–266.
- Sinclair, K.D., Farnsworth, R.W., Pham, T.X., Knight, A.N., Bloebaum, R.D., Skedros, J.G., 2013. The artiodactyl calcaneus as a potential "control bone" cautions against simple interpretations of trabecular bone adaptation in the anthropoid femoral neck. *J. Hum. Evol.* 64, 366–379.
- Skedros, J.G., Baucom, S.L., 2007. Mathematical analysis of trabecular "trajectories" in apparent trajectory structures: The unfortunate historical emphasis on the human proximal femur. *J. Theor. Biol.* 244, 15–45.

- Skerry, T.M., Lanyon, L.E., 1995. Interruption of disuse by short duration walking exercise does not prevent bone loss in the sheep calcaneus. *Bone* 16, 269–274.
- Skinner, M.M., Stephens, N.B., Tsegai, Z.J., Foote, A.C., Nguyen, N.H., Gross, T., Dieter, H., Pahr, D.H., Hublin, J.-J., Kivell, T.L., 2015. Human-like hand use in *Australopithecus africanus*. *Science* 347, 395–399.
- Spoor, F., Zonneveld, F., Macho, G., 1993. Linear measurements of cortical bone and dental enamel by computed tomography: Applications and problems. *Am. J. Phys. Anthropol.* 91, 469–484.
- Stern, J.T., 2000. Climbing to the top: A personal memoir of *Australopithecus afarensis*. *Evol. Anthropol.* 9, 113–133.
- Su, A., Carlson, K.J., 2017. Comparative analysis of trabecular bone structure and orientation in South African hominin tali. *J. Hum. Evol.* 106, 1–18.
- Su, A., Wallace, I.J., Nakatsukasa, M., 2013. Trabecular bone anisotropy and orientation in an Early Pleistocene hominin talus from East Turkana, Kenya. *J. Hum. Evol.* 64, 667–677.
- Susman, R.L., de Ruiter, D., Brain, C.K., 2001. Recently identified postcranial remains of *Paranthropus* and early *Homo* from Swartkrans Cave, South Africa. *J. Hum. Evol.* 41, 607–629.
- Tsegai, Z.J., Skinner, M.M., Pahr, D.H., Hublin, J.-J., Kivell, T.L., 2018a. Systemic patterns of trabecular bone across the human and chimpanzee skeleton. *J. Anat.* 232, 641–656.
- Tsegai, Z.J., Skinner, M.M., Pahr, D.H., Hublin, J.-J., Kivell, T.L., 2018b. Ontogeny and variability of trabecular bone in the chimpanzee humerus, femur and tibia. *Am. J. Phys. Anthropol.* 167, 713–736.
- Tsubota, K., Adachi, T., Tomita, Y., 2002. Functional adaptation of cancellous bone in human proximal femur predicted by trabecular surface remodeling simulation toward uniform stress state. *J. Biomech.* 35, 1541–1551.
- Vera, M.C., Ferretti, J.L., Abdala, V., Cointry, G.R., 2020. Biomechanical properties of anuran long bones: correlations with locomotor modes and habitat use. *J. Anat.* 236, 1112–1125.
- Volpatto, V., 2007. Morphogénèse des propriétés texturales du tissu osseux et environnement biomécanique: caractérisation non invasive du réseau trabéculaire et de l'os cortical du squelette appendiculaire de mammifères actuels et fossiles, hominidés inclus. Ph.D. Dissertation, Université de Poitiers.
- von Meyer, G.H., 1867. Die Architektur der spongiosa. *Arch. Anat. Physiol. Wiss. Med.* 34, 615–628.
- Vrba, E.S., 1975. Some evidence of chronology and palaeoecology of Sterkfontein, Swartkrans and Kromdraai from the fossil Bovidae. *Nature* 254, 301–304.
- Wallace, I.J., Tommasini, S.M., Judex, S., Garland, T., Demes, B., 2012. Genetic variations and physical activity as determinants of limb bone morphology: An experimental approach using a mouse model. *Am. J. Phys. Anthropol.* 148, 24–35.
- Wallace, I.J., Kwaczala, A.T., Judex, S., Demes, B., Carlson, K.J., 2013. Physical activity engendering loads from diverse directions augments the growing skeleton. *J. Musculoskelet. Neuronal Interact.* 13, 283–288.
- Wallace, I.J., Burgess, M.L., Patel, B.A., 2020. Phalangeal curvature in a chimpanzee raised like a human: Implications for inferring arboreality in fossil hominins. *Proc. Natl. Acad. Sci. USA* 117, 11223–11225.
- Ward, C.V., 2002. Interpreting the posture and locomotion of *Australopithecus afarensis*: Where do we stand? *Am. J. Phys. Anthropol.* 119, 185–215.
- Ward, C.V., 2013. Postural and locomotor adaptations of *Australopithecus* species. In: Reed, K.E., Fleagle, J.G., Leakey, R.E. (Eds.), *The Paleobiology of Australopithecus*. Springer, Dordrecht, pp. 235–245.
- Ward, F.O., 1838. *Outlines of human osteology*. Henry Renshaw, London.
- Whitehouse, W.J., Dyson, E.D., 1974. Scanning electron microscope studies of trabecular bone in the proximal end of the human femur. *J. Anat.* 118, 417–444.
- Wickham, H., 2009. *ggplot2: Elegant Graphics for Data Analysis*. Springer-Verlag, New York.
- Wolff, J., 1892. *Das Gesetz der Transformation der Knochen*. Hirchwild, Berlin.
- Zeininger, A., Patel, B.A., Zipfel, B., Carlson, K.J., 2016. Trabecular architecture in the STW 352 fossil hominin calcaneus. *J. Hum. Evol.* 97, 145–158.
- Zipfel, B., DeSilva, J.M., Kidd, R.S., Carlson, K.J., Churchill, S.E., Berger, L.R., 2011. The foot and ankle of *Australopithecus sediba*. *Science* 333, 1417–1420.